MULTIMODE MICROWAVE SENSORS FOR MICRODROPLET AND SINGLE-CELL DETECTION

A THESIS SUBMITTED TO
THE GRADUATE SCHOOL OF ENGINEERING AND SCIENCE
OF BILKENT UNIVERSITY
IN PARTIAL FULFILLMENT OF THE REQUIREMENTS FOR
THE DEGREE OF
MASTER OF SCIENCE
IN
MECHANICAL ENGINEERING

By
Hande Aydoğmuş
August 2018

Multimode Microwave Sensors for Microdroplet and Single-Cell Detection
By Hande Aydoğmuş
August 2018

We certify that we have read this thesis and that in our opinion it is fully adequate, in scope and in quality, as a thesis for the degree of Master of Science.

Mehmet Selim Hanay(Advisor)

Selçuk Yerci

Emine Yegân Erdem

Approved for the Graduate School of Engineering and Science:

Ezhan Karaşan
Director of the Graduate School

ABSTRACT

MULTIMODE MICROWAVE SENSORS FOR MICRODROPLET AND SINGLE-CELL DETECTION

Hande Aydoğmuş
M.S. in Mechanical Engineering
Advisor: Mehmet Selim Hanay
August 2018

A novel detection mechanism which can reveal both morphological and electrical properties of analytes are needed for Lab-on-a-Chip applications. Herein, a label-free, real-time and non-contact detection paradigm in microwave domain is constructed, by using first and second electromagnetic modes of a microwave resonator. As the resonator, microstrip line is chosen since it offers accessible boundary conditions. In order to deliver the analytes into the sensing region, microfluidic channels are fabricated. As a proof-of-concept, while the microstrip line resonator's first and second modes are tracked simultaneously, analytes are delivered through the microchannel embedded underneath the signal layer. As the analytes, water microdroplets in oil, cervical (HeLa) and breast (MDA-MB-157) cancer cells in their appropriate medium are used and detected; their position and electrical volume informations are obtained and compared. Allan Deviation of the measurement is smaller than 2×10^{-8} for both modes, and due to analyte properties in microwave domain, such as the great permittivity difference between the biological analyte and medium, detection is possible.

In order to test the accuracy of finding the position of the analyte, two different microchannel geometries are designed. The first geometry is based on a zigzag channel, where microstrip line crosses the channel at 6 different locations. Secondly, a branched channel is designed, to send the microdroplets at four different locations. This delivery mechanism is mostly based on the hydraulic resistance: Each droplet chooses its path by the hydraulic resistance that is caused by the previous droplet. Hence, microdroplets are distributed to four channels. Due to the mode shape of the specific mode, when analyte passing through these regions, it induces different frequency shifts. For these applications, microfluidic part is fabricated by conventional soft lithography methods, and the material for the microchannels is PDMS. Electrical volume of the droplets is also obtained.

After the usage of prototypes for position and electrical volume calculations, second generation devices are fabricated. Compared to the PDMS-based devices, these devices offer rapid and low-cost prototyping. Additionally, Kapton is chosen for the dielectric material, and it has some material-wise benefits, such as the tangent loss level. Analytes are delivered through the sensing region by capillary tubings, hence soft lithography steps can be eliminated. Due to the equipment limitations, only the first mode is tracked with these novel devices, while another type of breast cancer cells (SK-BR-3) are delivered through the sensing region. Signal-to-noise ratio, when compared to the PDMS based devices, is improved.

In this work, the first two modes of microstrip line resonators are used. However, by using higher order modes, more properties about the particles as skewness, geometrical volume, orientation, and composition can be obtained. These informations can be used to construct a global image of the analyte; rather than a pixel by pixel image. Additionally, flow cytometry applications, detection of Circulating Tumour Cells and applications for long term cultivation on chip (also known as Organ-on-Chip platforms) can be achieved.

Keywords: Microwave Resonators, Microfluidics, Lab-on-a-Chip Applications, Biosensors, Multimode Detection.

ÖZET

ÇOK MODLU MİKRODALGA SENSÖRLERİ İLE MİKRODAMLACIK VE TEK HÜCRE SAPTANMASI

Hande Aydoğmuş
Makine Mühendisliği, Yüksek Lisans
Tez Danışmanı: Mehmet Selim Hanay
Ağustos 2018

Parçacıkların morfolojik ve electriksel özelliklerini tespit edebilen yeni sistemler, Çip Üstü Laboratuvar Uygulamaları için gereklidir. Bu çalışmada, mikrodalga alanında, gerçek zamanlı, temassız ve etkitetleme ihtiyacı doğurmayan bir tespit etme yaklaşımı; bir mikrodalga rezonatörünün ilk ve ikinci elektromanyetik modları, kullanılmıştır. Sınır şartları dolayısıyla, mikroşerit hatlı bir rezönatör seçilmiştir. Parçacıkları algılama bölgesine ulaştırmak için mikrokanallar üretilmiştir. Kavramı kanıtlamak için rezönatörün ilk ve ikinci modu aynı anda sürülürken, parçacıklar, sinyal hattının altındaki bu mikrokanalları kullanarak algılama bölgesine gönderilmiştir. Parçacık olarak yağ içinde su mikrodamlacıkları; uygun besiyeri içindeki rahimağzı (HeLa) ve meme kanser hücreleri (MDA-MB-157) kullanılmış ve saptanmıştır; bu parçacıkların pozisyon ve elektriksel hacim özellikleri elde edilmiştir ve karşılaştırılmıştır. Allan Sapması değeri iki mod için de 2×10^{-8} değerinden az olup, mikrodalga rejiminde madde özellikleri dolayısıyla; örneğin biyolojik parçacık ve parçacığa özel besiyeri arasındaki büyük elektriksel geçirgenlik farkı, tespit etme mekanizmasını mümkün kılmıştır.

Sistemin pozisyon bulma algoritmasındaki doğruluğunu test etmek için, iki farklı mikrokanal geometrisi dizayn edilmiştir. İlk geometri, zigzag şeklindedir ve sinyal hattı ile altı farklı lokasyonda karşılaşmaktadır. İkinci geometri ise dört kola ayrılmaktadır ve mikrodamlacıkları dört farklı lokasyona göndermek için tasarlanmıştır. Bu gönderme mekanizması hidrolik direnç mekanizmasını temel alarak çalışır: Her damlacık gideceği kanalı ondan bir önce giden kanalın yarattığı hidrolik dirence göre belirler, böylelikle dört kanala da damlacık dağılımı gözlemlenmiş olur. Parçacık sinal bölgelerinden geçerken göz önünde bulundurulan her modda farklı bir frekans kaymasına sebep olur. Bunun sebebi de her modun, ayrı bir

mod şeklinin olmasıdır. Bu uygulamalardaki mikrokanal kısmı mikroakışkanlarda yaygın kullanılan litografi metodu ile üretilmiştir ve mikrokanalların üretiminde PDMS maddesi kullanılmıştır. Mikrodamlacıkların elektriksel hacmi de hesaplanmıştır.

Prototip aletler pozisyon ve elektriksel hacim hesaplamalarında kullanıldıktan sonra, farklı cihazlar da dizayn edilmiş ve üretilmiştir. Bu yeni jenerasyon cihazların ilk modellerden en büyük farkı ise daha ucuza ve daha hızlı üretilmeleridir. Ayrıca, dielektrik materyal olarak Kapton seçilmiştir ve Kapton'un kayıp tanjantı değeri başta olmak üzere bazı üstün materyal özellikleri bulunmaktadır. Parçacıklar algılama bölgesine kapiler boru ile gönderilmiştir; böylelikle litografi metodu ve diğer fabrikasyon yöntemlerine duyulan ihtiyaç ortadan kaldırılmıştır. Kullanılan ekipmanların çalışma limitlerinden dolayı, yeni nesil cihazlarda sadece ilk mod sürülmüştür ve denemek için başka bir tür meme kanseri hücresi (SK-BR-3) saptanmıştır. Önceki aletlerle karşılaştırıldığında, sinyal gürültü oranında bir iyileşme gözlemlenmiştir.

Anlatılan çalışmada mikroşerit hatlı rezönatörün ilk iki mod kullanılmıştır. Bununla birlikte, üst seviye modlar kullanılarak parçacıklarla ilgili daha çok bilgi; geometrik hacim, eğrilik, oryantasyon, parçacığın bileşimi, elde edilebilir. Pikselli görüntü alımındansa bu bilgiler ile parçacığın global görüntülemesi elde edilebilir. Ek olarak bu sistem, akışlı hücre sayımı aplikasyonlarında, dolaşımdaki tümör hücrelerinin saptanmasında ve uzun dönem çip üstü hücre kültürleme araştırmalarında (bu platformlar Çip-üstü-Organ olarak da bilinmektedir) kullanılabilir.

Anahtar sözcükler: Mikrodalga Rezonatörleri, Mikroakışkanlar, Çip Üstü Laboratuvar Uygulamaları, Biyosensörler, Çok Modlu Algılama.

Acknowledgement

I sincerely want to thank my advisor, Dr. Selim Hanay, who taught me the meaning of interdisciplinary science. Without Dr. Hanay, I would not be this scientist who has a mechanical engineering degree, and working with cancer cells and I cannot thank enough for his support, knowledge, and guidance. I wouldn't have learnt this much, if I was not working with you sir. I am thankful to my MS thesis committee, Dr. Yegân Erdem and Dr. Selçuk Yerci for their valuable time.

Hanay Research Group; each of you taught me so many stuff -whether or not related to our research-, and it is a privilege to work with you. Ezgi Orhan, Levent Aslanbaş, Arda Seçme, Utku Hatipoğlu, thank you for your valuable contributions, exchange of ideas. Selçuk Oğuz Erbil, thank you for your close friendship and all the times we spent in the cleanroom, trying to fabricate the best chips. Mert Yüksel, thank you for your help, close and thoughtful friendship; and all the coffee we had. Mehmet Kelleci, I cannot thank you enough. Where should I begin? This work would not be where it is without you, and you taught me so much. You are the best "lab-mate" anyone could have and it is an honour to be in the same project with you. You are more than a brother to me, and always the companion in misfortune. Finally, our alumni, Çağatay Karakan and Atakan Bekir Arı, thank you for your guidance and friendship.

Irmak Ulusoy and Barış Topçu, my dearest friends, thank you for your support, and being there for me, all the time. All the graduate students at the Department of Mechanical Engineering; Ozan Temiz, Müge Özcan, Cem Kurt, Dilara Uslu, Levent Dilaveroğlu, Hammam Mohamed; thank you all for the moral support, I hope which is mutual, it is a privilege to walk on the same road with you. Onur Vardar, thank you for being one of the closest friends, and valuable discussions.

I want to express my gratefulness to my family. My dad, Teo, a dedicated engineer who has influenced me the most in this path. Mum, there is not enough words to explain my love, my gratitude. I (hope to) believe I got your work ethics,

thanks to the sleepless nights in the gynaecology clinic, when you were working for limitless hours. My sister, my best friend, Zeynep, literally I would not be this person without you. Even though we have moved to two different continents, I feel your unconditional love and support, on every subject. Without you guys, I would not be this scientist who is trying her best.

Finally, women in engineering and science, please do not hesitate to improve yourselves to become your better versions, always work hard, and believe in yourselves. “We can do it.”

Contents

1 Introduction **1**

1.1 Microfluidics and Lab-on-a-Chip Devices 2

1.2 Mechanical Domain 5

1.2.1 Inertial Imaging 5

1.2.2 Suspended Microchannel Resonators 6

1.3 Analogy Between Mechanical and Microwave Domains 7

1.4 Microwave Resonators Integrated with Microfluidics 7

1.5 Thesis Outline 9

2 Microwave Domain **11**

2.1 Imaging in Microwave Domain 11

2.1.1 Theory Behind Imaging 13

2.1.2 Measurement Devices, Circuit and Two Mode Tracking . . 16

3 Fabrication of Microstrip Line Resonators with Microchannels **19**

3.1 Sample Preparation 19

3.2 Soft Lithography 20

3.2.1 Mask Preparation 21

3.2.2 Preparation of the Master 21

3.2.3 PDMS Preparation 25

3.2.4 Ground & Strip Layers 26

4 Droplet Detection with Microstrip line Resonator 30

4.1 Droplet Microfluidics 31

4.1.1 Capillary Number 31

4.1.2 Flow Rate Ratio 32

4.1.3 Geometry 33

4.1.4 T-Junction for Droplet Formation 33

4.2 Droplet Detection with a Zigzag Microchannel 34

4.3 4-Branched Microchannels for Droplet Distribution, Location and Electric Volume Calculations 36

5 Cancer Cell Detection & Differentiation 40

5.1 Cell Detection 43

5.1.1 Electrical Volume Difference 45

5.2 Wild Type and Drug Resistant Breast Cancer Cells 47

6 Novel Facile Resonators **49**

6.1 Fabrication 50

6.2 Cell Experiment 51

6.3 Kapton Etch Trials 52

7 Conclusion and Future Works **57**

7.1 Organ-on-Chip Platforms 58

7.2 Fused Silica Device Fabrication 61

A Cell Culture **71**

A.1 Cell Medium Composition 71

A.2 Cell Culturing Equipments 72

B Droplet Formation Simulations **73**

List of Figures

2.1 Schematic of microstrip line resonator with microchannel. First and second modes and mode shapes are indicated. 12

2.2 Schematic of the circuit which is used for simultaneous two modes tracking of the microwave resonator. 17

2.3 Schematic of PLL circuit; measurement system for each mode. Reprinted with permission of Royal Society of Chemistry, Lab on a Chip Journal, Issue 3, 2018. 18

3.1 Photomasks for microfluidic applications. 21

3.2 Schematic of photolithography onto negative photoresist. 23

3.3 Si wafer with SU-8 structures; in this case a 8-branched microchannel. To use only 4-channels, a portion of SU-8 is removed from the mask. 25

3.4 Si wafer with SU-8 structure; namely a single microchannel geometry. Width of the channel is approximately $50\mu m$. 25

3.5 Silicon with SU-8 structures. A thin layer of PDMS is poured and baked. 26

3.6 Final products for different applications. Coloured DI water is filled in order to embellish the microchannels. 27

3.7 Fabrication schematic of the device. 28

3.8 Final product for a device with a zigzag microchannel. 28

3.9 Port connector with epoxy. 4 branch of microchannels and microstrip are also visible. 29

4.1 T-Junction for droplet formation. Water droplets are formed with carrier fluid, oil. 34

4.2 Frequency shifts on first and second modes due to droplet passage. Point E is approximately at the center of the device. 35

4.3 (a)4 microchannels that are used for droplet distribution. (b)Histogram of 121 droplets and their choice of microchannels. (c)Frequency shifts on both modes, due to droplet passage from one of the channels, A to D. 37

4.4 Droplet sorting by branching the microchannels. Two droplets are visible. Second droplet favours channel with lower hydraulic resistance. 38

4.5 Position data of the droplets in frequency shift domain. Inset also shows how position and electrical volume contours are calculated. Reprinted with permission of Royal Society of Chemistry, Lab on a Chip Journal, Issue 3, 2018. 38

4.6 Droplet information. Reprinted with permission of Royal Society of Chemistry, Lab on a Chip Journal, Issue 3, 2018. 39

5.1 HeLa cells' histogram. Inset image shows microscopy image of HeLa cells. 41

5.2 MDA-MB-157 cells' histogram. Inset image shows microscopy image of the same cells. 41

5.3 Control runs for Allan Deviation calculations. Response time of both modes can be observed. Reprinted with permission of Royal Society of Chemistry, Lab on a Chip Journal, Issue 3, 2018. 43

5.4 Allan Deviation plots for the first and second modes. 44

5.5 Frequency shifts on both modes due to HeLa passage. 44

5.6 Frequency shifts on both modes due to MDA cells' passage. 45

5.7 Frequency shifts on both modes due to a group of HeLa cells. . . 45

5.8 Electrical volume histogram of HeLa cells and microdoplets. Outliers indicate entry of multiple cells into the channel at the same time. The inset compares the size of the HeLa cells to the size of the microdroplets. 46

5.9 Electrical volume comparison of the HeLa and MDA-MB-157 cell lines. Reprinted with permission of Royal Society of Chemistry, Lab on a Chip Journal, Issue 3, 2018. 46

5.10 Optical microscopy images of breast cancer cells. 47

5.11 Size comparison of wild type and treated breast cancer cells. Since they are similar in size, it is difficult to compare their electrical volume. 48

6.1 Microstrip line resonator with Kapton and capillary tubings. . . . 50

6.2 Frequency shifts on first mode due to single cell passage events. . 51

6.3 Allan Deviation of the first mode. 52

6.4 First mode frequency shift histogram. 52

6.5 Optical microscopy images of etching where SU-8 is used as the masking material. 54

6.6 SEM image of etching from different perspectives. 54

6.7 SEM images of etching when the chrome is used as the masking material. 56

7.1 Microscope inside an incubator, surrounded by faraday cage. . . . 61

7.2 Schematic of fused silica sample after inlet-outlet openings and lithography. 62

7.3 Schematic of the sample with ground layer and microchannel. . . 63

B.1 Droplet formation trial while V_{water} is greater than V_{oil}. 74

B.2 Droplet formation trial while V_{water} is smaller than V_{oil}. 74

B.3 Droplet formation with different velocity ratio. 75

List of Tables

3.1 Spin Coating Parameters for 200μm Resist 22

3.2 Spin Coating Parameters for 75μm Resist 22

3.3 Photolithography Parameters 24

3.4 Photolithography Parameters for 75μm thickness of SU-8 24

4.1 Flow Rates of the Continuous and Dispersed Flows 33

4.2 Normalized Positions of the Microchannel Sections Where They Cross the Signal Line. 35

6.1 Spin Coating Parameters for 40μm Resist 53

Chapter 1

Introduction

This thesis introduces a novel detection mechanism in microwave domain, which is integrated with microfluidics. As a laboratory whose work is mostly in mechanical domain and Nanoelectromechanical Sytems and their vibrational modes, moving to microwave domain was not a burden due to the analogy between mechanical and microwave domains. In this work, a microstrip line resonator is fabricated with a microfluidic channel embedded between its signal and ground layers. In theory, while the microwave resonator's higher order electromagnetic modes are tracked simultaneously, and if an analyte is delivered to the sensing region, morphological and electrical properties of this analyte can be extrapolated. These kind of Lab-on-a-Chip devices are needed especialy for biological experiments, since biological analytes which are needed to be sensed should be in appropriate medium, in order to maintain their viability. For this work, first two electromagnetic modes are tracked, and position and electrical volume of the analyte are gathered. As a proof-of-concept, first experimental trials are done with water microdroplets in oil. Due to permittivity difference, simultaneous frequency shifts on both modes are observed. In order to study position calculations, different microchannel structures are designed and fabricated. Secondly, HeLa (cervical) and MDA-MB-157 (breast) cancer cells are tracked. Each single cell causes frequency shifts on all considered modes. Their electrical volumes are also differentiated. Even though there is a great volume difference (orderwise) between the resonator

itself and the analyte which is desired to be sensed, namely cancer cells; Allan Deviation results which are lower than 2×10^{-8} and microwave frequency range make sensing possible.

First prototype resonators' microfluidic parts are based on PDMS and soft-lithography techniques. Another prototype is also developed, which is based on capillary tubings. This new type of devices are low-cost, and can be rapidly produced. With this detection mechanism, label-free and real-time detection of biological analytes, namely cancer cells can be achieved.

With multi-mode sensing techniques, rather then pixel by pixel imaging, global image of the analyte can be constructed. This label-free and real-time sensing platform offers characterization of cells, and in the future, it can be used for flow cytometry applications, analysing the composition of biological particles, or detection of Circulating Tumour Cells.

1.1 Microfluidics and Lab-on-a-Chip Devices

Fabrication of microsystems began as early as in the late 1960s, with advancement in nano-micro fabrication techniques. Microfluidic technologies, with various advantages, as using small volumes of samples, short times of analysis, low cost, carrying out chemical reactions with high resolution and sensitivities[1], and capability of integrating different life sciences, evolved from microsystems. Microfluidics involved in different branches. First applications of microfluidics include chromatography platforms. In 1990s, defense industries aimed to deploy microfluidics for chemical and biological threat detectors in warzones. Another application was the first trial of the ink-jet printing technology[2]. Additionally, biological applications as DNA sequencers[3] had been introduced, as rapid platforms compared to their macro-sized counterparts.

With the advancement in microfluidic technologies, researchers have started to integrate systems in one chip. Depending on the application, this chip includes

microchannels, electronic parts for transduction and read-out, mixers, pumps, valves. Hence, it abolishes the need for major equipments, and the chip itself gathers laboratory techniques into a system. This is how microfluidics evolved to lab-on-a-chip; not just the microchannels, but necessary systems to extract data for various applications are included in this major field. Of course, researchers should have a focus on some requirements when developing a new LoC system, as being sensitive, low cost, compact, and the test that take shorter time to result then macro counterparts[4].

Moving from macro to micro scale has specific advantages. One of the main advantage is that capillary forces become more dominant, and passive fluidic actuation becomes favourable[5]. *Reynolds Number*, a dimensionless number which is the ratio of inertia force to viscous force, therefore which specifies the flow regime, can be used to characterize whether the flow is in the laminar or turbulent regime.

$$Re = \frac{\rho u L}{\eta} \tag{1.1}$$

Where ρ is the density of the fluid, u is the velocity of the fluid, L is the characteristic length, and η is the dynamic viscosity of the fluid. In microfluidics, due to its dimensions, flow is usually described with small Re; therefore in laminar regime. If Navier-Stokes equation is also investigated in micro domain for newtonian and incompressible fluid flow:

$$\rho(\frac{\partial(u)}{\partial t} + u.\nabla u) = -\nabla p + \eta\nabla^2 u \tag{1.2}$$

Which can be interpreted as acceleration terms versus the force terms. The first term implies the acceleration due to unsteadiness, second term is the convective acceleration of the velocity field, third term is the pressure gradient, and final term is the viscous force. At micro scale, assuming unidirectional steady fluid flow, the equation becomes Stoke's equation:

$$\nabla p = \eta\nabla^2 u \tag{1.3}$$

This equation gives no time dependence, which will result in instantaneous

changes in the flow. Laminar flow also shows some characteristics as being linear, reversible, steady and independence from inertia. Hence, microfluidics have unique properties, which result in well-defined and stable liquid-liquid interfaces, due to smaller dimensions. Thus, even at single cell level effects can be examined [5].

As it is mentioned above, cell studies gain importance with LoC devices. How cells behave inside human body is the main question for *Point of Care* applications. These applications try to investigate different drug delivery systems, diagnosis, and how every individual responses to different types of drugs. The main goal is to develop a portable low-cost instrument, a real Lab on a Chip, in order to get rid of expensive lab equipments, and to especially reach to people in rural settlements. An example for a point of care device is the cell counting and sorting platform, a flow cytometer, which consists of a disposable microfluidic chip, and a miniaturized detection system [6].

For biological studies, cell to cell as well as cell to extracellular matrix interactions have being investigated. There are different research groups that examine cell growth rates by mimicing complex extracellular matrix [7], isolation of individual cells by using microfluidic sorting devices with appropriate biological assays [8], or use impedance sensing with dielectrophoretic cages to manipulate microorganisms, without any chemical labeling [9].

As it can be examined, microfluidics and Lab-on-a-Chip devices have various applications, and in the beginning of 2000s, biomicrofluidics gained a different perspective, especially with the development of single cell sorting, monitoring, and manipulating platforms. After nearly 18 years, these devices still have great potential, yet to be discovered, to solve diagnostic problems, to gain a sight for various types of tumour cells.

In this work, microfluidics are used for droplet forming and sorting, and cell delivery to the sensing area. These parts will be discussed in detail, on the following sections.

Cells are cultured in petri dishes, and these dishes do not mimic their natural environment; human body. Organ-on-chips, namely cell culturing platforms that try to mimic a part of a tissue or an organ, by using microfluidics. These platforms are especially important to understand how a drug affects that specific cell group, and cells do react differently in situ. Organ on chips will also be covered in the Future Works Section, in order to investigate how our system can be integrated with these kind of platforms.

1.2 Mechanical Domain

In this section, mechanical domain refers to the vibrational modes of resonators, Nano an micro electromechanical systems, and how information about analytes can be extracted by using these platforms.

1.2.1 Inertial Imaging

Nano and micro resonators are used for weighing analytes of different size and composition ranging from gold nanoparticles to bacteria and they may be used to detect biological analytes such as live cells [10].

When an analyte lands on a nanomechanical resonator, for instance on a double-clamped beam, it will induce frequency shifts, depending on the mass and position of the analyte, on each corresponded mechanical modes.

By using multiple vibrational modes of a resonator, spatial information of analytes as mass, shape and size can be obtained, in real-time. After obtaining these spatial properties, an image can be constructed. This reverse imaging algorithm is known as *Inertial Imaging* [11]. Since fluctuations of the frequency response give the resolution, ultrasensitive measurements are achievable.

1.2.2 Suspended Microchannel Resonators

As it is explained, nano and micro resonators can be used to obtain spatial properties of biological analytes. It is desirable to examine the characteristics of biological particles as cells in a suitable solution, to maintain their viability. However, when resonators are surrounded with fluid, viscous damping of the fluid degrades quality factor, resulting in low sensitivity.

In 2003, a research group from MIT came out with the idea of *Suspended Microchannel Resonators*, SMR, in which the fluid channel is inside the resonator, kept at vacuum. SMR are excited on their higher modes, simultaneously, to extract information about particles. They eliminated viscous damping effects, hence obtained high quality factors and high sensitivity [12]. The first experiments were detection of the binding of avidin and biotinylated bovine serum albumin, in real-time. They continued with measuring individual particle masses with femtogram resolution [13], weighing bacterial cells, with high quality factor (15,000) resonators, without binding [10], density characterization of human red blood cells and E.Coli [14], density differentiation of two different cancer cell lines by using dual-SMR[15].

Apart from single cell studies, cell growth rates are also being studied. These studies have major impact, since they are directly related to drug susceptibility testing, as it is explained at Microfluidics and Lab-on-a-Chip Devices Section. They are weighing cells; namely mouse and human T cells, repeatedly while flowing cells from the microfluidic channel with several resonant mass sensors. They obtain cellular responses of cells to antibiotics [16]. At another study, they are measuring the mass accumulation rate of tumour cells, MAR, in order to investigate the drug sensitivity for every individual patient, and single cell therapeutic responses [17]. Drug sensitivity of single multiple myeloma cells are also examined by using MAR. Due to the high rates of drug resistance, finding the most effective theraphy is needed [18].

As it can be examined, micro and nano resonators have being used widely, for various applications. However, there are some drawbacks. Especially, the

fabrication of Suspended Microchannel Resonators is challenging; etching microfluidic channels on silicon, or anodic bonding to enclose them. Moving from mechanical domain to electromagnetic domain can expedite the fabrication process. Additionally there are similarities between these two domains, and they will be investigated at the next section.

1.3 Analogy Between Mechanical and Microwave Domains

Inertial Imaging principles, developed for NEMS, can be extended to electromagnetic resonators as well. Higher-order modes of microwave sensors have not being used for extracting morphological properties. However, in mechanical domain, micro and nanomechanical sensors have been driven in their higher-order modes to obtain information as measuring mass and stiffness of particles [19], weighing particles in real time [11], and getting spatial properties to form inertial imaging of the particle [20], as stated above.

While an analyte travels through the sensing region, it causes frequency shifts in all considered modes, similar to mechanical domain. These frequency shifts depend on the analyte, and the mode shape. When the frequency shifts from all modes considered, global properties of the analyte can be extracted. These features can be electrical volume, position, and shape of the analyte. Hence, global image of an analyte can be extracted.

1.4 Microwave Resonators Integrated with Microfluidics

Microwave resonators have being used with fluidics for different applications. One of the early applications is the characterization of different liquids by comparing

dielectric properties by using coplanar sensors[21]. However, this integration is not with in micro-scale, but with greater volume of liquids. Similar application with smaller volumes of liquid, on the order of nanoliter, has been investigated after almost a decade from aforementioned work [22]. Some of the microwave resonators for dielectric property characterization of liquids do not need expensive equipment for fabrication; instead, resonator can be integrated with capilary tubings [23]. Additionally, concentration characterization can be achieved, and researchers have investigated the glucose concentration in water, by measuring the resonance property of the resonator, with a microstrip line resonator [24]. Especially with the technological improvement of micro-nano fabrication techniques, biological applications, bio-sensors, gain a momentum as well. By using a HF-based sensing technique, a coplanar waveguide platform, researchers have shown label-free, contactless detection for biological analytes, namely human umbilical vein endothelial cells, by using micro-liter volumes of liquid [25].

In order to develop an electronic sensing platform for biological analytes, ions in cell medium should be taking into consideration, since they will compose electrical double layer [26]. This double layer causes sensing problems at low frequency domain; however, at microwave band, electromagnetic sensing is not limited by Debye screening [27]. Therefore, microwave sensors, resonators, can be used as a label-free biosensing platform for biological analytes, and morover single cell detection can be achieved. Researchers have shown that baker's yeast (Saccharomyces cerevisiae) and Chinese hamster ovary cells can be detected in suspending fluids as phosphate-buffer saline by microwave resonator integrated with an interferometer [28].

In the works that are mentioned above, generally network analyzers are used. Network analyzers are used to test designs which are in the RF or microwave regime by measuring their response. In our work, network analyzer is only used to characterize the initial values. First two modes of the resonator are tracked by a system that is designed for real-time and sensitive measurement.

1.5 Thesis Outline

Chapter 1 gives information about microfluidics and Lab-on-a-Chip platforms, sensing in mechanical domain; namely mass spectrometry, inertial imaging. It moves on to suspended microchannel resonators, devices with embedded microfluidic channels to obtain mass, size, density information about biological analytes, without getting affected by viscous damping of the fluid which carries these analytes. These resonators are excited in their vibrational modes, and despite the fact that they have various applications and high sensitivity levels, fabrication of such devices is a drawback. This chapter continues with the analogy between mechanical and microwave domains, and concludes with some examples in the literature which use microwave resonators integrated with microfluidics.

In Chapter 2, microwave imaging is introduced. This novel platform is a variation of inertial imaging from mechanical domain, in order to obtain morphological and electrical properties of analytes.

In Chapter 3, fabrication of microstrip line resonators integrated with microfluidics is explained. Fabrication has various steps, both in the cleanroom and in the lab environment. Basically, it is a combination of soft lithography and device bonding.

In Chapter 4, droplet microfluidics and how it is implemented to microwave imaging is investigated. Two different types of microchannels are fabricated; zigzag and 4-branched. Zigzag microchannel is used to detect water microdroplets in oil, and branched microchannel is used to characterize droplets' position and electrical volume, while they are passing through the sensing region.

In Chapter 5, different cancer lines, cervical (HeLa) and breast (MDA-MB-157) are used for microwave imaging. Detection of cells and electrical volume differentiation is presented.

In Chapter 6, novel microstrip line resonators are introduced. These devices are based on Kapton, and do not need any cleanroom process or equipment.

They are low-cost, easy and fast to produce. Experiments are done with SK-BR-3 breast cancer cells, with the first mode of the resonator.

In the final chapter, conclusion of the work is presented and future works are discussed. These platforms can be integrated with Organ-on-Chips to further investigate drug susceptibility, resistance or to study cell-to-cell interactions.

Chapter 2

Microwave Domain

In this work, resonators which work in microwave regime are used. Microwave band is named for electromagnetic waves between 1GHz to 300GHz frequencies. The reason to use these type of resonators is due to the fact that these type of short wavelengths offer some advantages, and these advantages are explained in this section.

Microwaves radiate electromagnetic energy, travel in straight lines, and they are reflected by conducting surfaces. Waves propagate through transmission lines, by transmitting energy. Basically, transmission lines can be divided into two groups: Multiconductor Lines and Waveguides; which are Single Conductor Lines. There are some differences between multiconductor lines and waveguides, as supporting TEM wave, having a cut-off frequency or not, amount of reflections, dispersion of waves and limitations on bandwidth. In the works presented here, microstrip line resonators, which are in the multiconductor lines group, are used.

2.1 Imaging in Microwave Domain

New detection techniques in microwave regime offer some potential by being compact, low-cost, and sensitive. These electronic sensing techniques are integrable,

and in this work, microstrip line resonators integrated with microfluidics are used to obtain morphological and electrical properties of anayltes; namely water micro-droplets in continuous oil, and various cancer cells in their appropriate medium. Morphological properties such as position and shape of an analyte can be extracted by using higher-order modes of the sensor. Once these informations are available, global image of the analyte can be constructed.

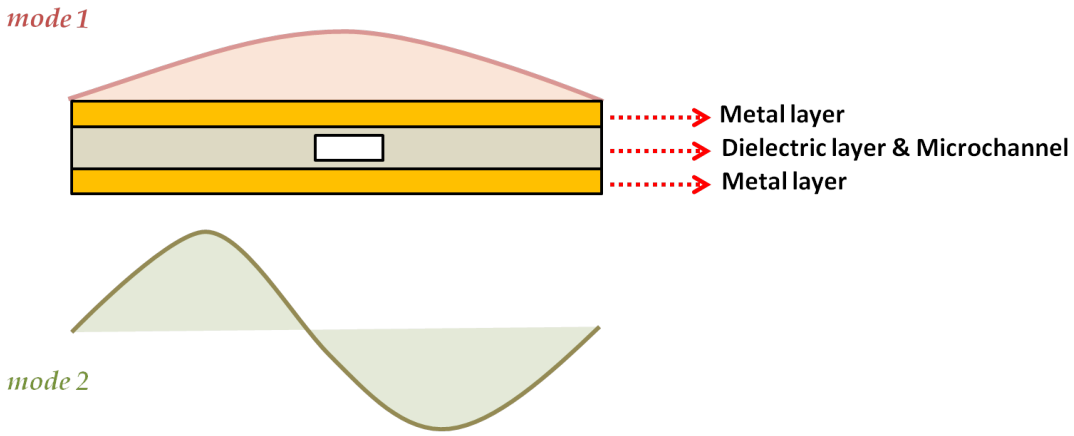

Figure 2.1: Schematic of microstrip line resonator with microchannel. First and second modes and mode shapes are indicated.

As it is explained at Chapter 1, integration of microwave resonators with microfluidics, microwave regime has some unique properties. One of them is the fact that Debye screening is not a limitation, as in the case of low frequency applications.

Permittivity of materials depend on temperature and frequency. For instance, water has a permittivity around 80 below 3GHz, and it decreases with increasing frequency [29].If biological analytes is taken into account, as proteins (4-6, below 3GHz), one can observe the contrast between relative permittivity values at the microwave regime [30]. To give different information about biological tissues, one can examine [31] and [32]. One thing in common is the relative permittivity values for these tissues, ranging from bone to kidney, are around 10. Hence, this contrast between biological particles and medium that carry them makes microwave imaging favourable, since at optical frequencies, refraction of biological materials and carrier fluids are similar.

2.1.1 Theory Behind Imaging

When there is a change in the permittivity of the dielectric material, in this case due to the passage of an analyte through microchannel embedded inside the microstrip line resonator, it causes frequency shifts. These frequency shifts, denoted with Δf_n, are related to ε; dielectric constant of the medium, μ; permeability of the medium, E_n and H_n are the electrical and magnetic field for the n_{th} mode.

$$\frac{\Delta f_n}{f_n} = -\frac{\int_{V_0} \Delta\varepsilon(r) E_n^2(r) d^3r}{\int_{V_0} (\varepsilon(r) E_n^2 + \mu(r) H_n^2) d^3r} \tag{2.1}$$

The equation can be simplified further by taking into consideration at resonance condition, since right hand side denominator is the total stored energy of the resonator:

$$\left\langle \int \varepsilon E_n^2 d^3r \right\rangle = \left\langle \int \mu H_n^2 d^3r \right\rangle \tag{2.2}$$

After substituting harmonic oscillator property, the frequency shift equation becomes:

$$\delta f_n = -\frac{\int_{V_0} \Delta\varepsilon(r) \phi_n^2(r) d^3r}{2\int_{V_0} \varepsilon(r) \phi_n^2 d^3r} \tag{2.3}$$

Where the left side is the fractional frequency shift. The denominator can be thought as the effective electrical volume of the considered mode, V_n, and the equation becomes:

$$\delta f_n = -\frac{\int_{V_0} \Delta\varepsilon(r) \phi_n^2(r) d^3r}{2V_n} \tag{2.4}$$

If the analyte is thought as a point particle, where its shape or size is arbitrary in the given context, dirac delta function can be taken into account. Therefore,

$\Delta\varepsilon(r)$ becomes:

$$\Delta\varepsilon(r) = \nu\delta(r - r_p) \tag{2.5}$$

Where ν is the excess electrical volume, and r_p is the position of the point particle. If the dielectric constant is replaced:

$$\delta f_n = -\frac{\nu\phi_{r_p}^2}{2V_n} = -\frac{\nu\phi_x^2}{2V_n} \tag{2.6}$$

As it is explained above, in this work microstrip line resonators are used. These resonators are one-dimensional, hence frequency shifts for the first two modes can be simplified into:

$$\delta f_1 = -\frac{\nu\phi_1(x)^2}{2V_1} \tag{2.7}$$

$$\delta f_2 = -\frac{\nu\phi_2(x)^2}{2V_2} \tag{2.8}$$

These two equations leave two unknowns, namely ν and ϕ.

As it can be examined from the equations above, frequency shifts are proportional to the square root of the electric field. Fringing fields can be neglected, since active region is directly under the microstrip line, at z direction. Thus local electric field equation can be written with amplitude A_n and mode shape, ϕ_n, in the z direction.

$$E_n(r) = A_n\phi_n(x)\tilde{k} \tag{2.9}$$

As it will be investigated further on the upcoming sections, microstrip lines used in this work are shorted from both ends, creating boundary conditions.

Hence the mode shape function can be expressed with $\phi_n = sin(n\pi x)$, and this function can be replaced in the main equation. Hence the electrical volume of a particle can be calculated with:

$$\delta f_n = -\frac{\nu \sin^2(n\pi x)}{2V_n} \tag{2.10}$$

To find the location of the particle, after excess electrical volume is known, $deltaf_1$ and $deltaf_2$ can be substituted. By using only half of the device:

$$\frac{\delta f_2}{\delta f_1} = -\frac{\sin^2(2\pi x)}{\sin^2(\pi x)} \tag{2.11}$$

$$\frac{\delta f_2}{\delta f_1} = -\frac{4\sin^2(\pi x)\cos^2(\pi x)}{\sin^2(\pi x)} \tag{2.12}$$

$$\frac{\delta f_2}{\delta f_1} = -4\cos^2(\pi x) \tag{2.13}$$

Finally;

$$x = \frac{1}{\pi}\arccos\left(\sqrt{\frac{\delta f_2}{\delta f_1}}\right) \tag{2.14}$$

In conclusion, by using the first two modes of the microstrip line resonator, an analyte passing through inside the microchannel, which is embedded inside the resonator, position and electrical volume calculations can be done.

To verify the experimental results of electrical volume and position, Maxwell-Garnett approach can be used. This approach allows to approximate effective permittivity, since it concerns the host medium, and replacement of this medium by another media. In the equation, ε_i is the permittivity of the disperse flow (water for droplet experiments or cells for cancer cell detections), ε_h is the permittivity of the carrier flow (oil for droplet experiments, cell medium for cell

detections), and f is the filling ratio, which explains the quantitative change of the disperse and continuous liquids.

$$\Delta\varepsilon = 3f\varepsilon_h \frac{\varepsilon_i - \varepsilon_h}{\varepsilon_i + 2\varepsilon_h} \tag{2.15}$$

2.1.2 Measurement Devices, Circuit and Two Mode Tracking

As it is explained in the Introduction Chapter, network analyzer is only used for the first characterization of the device. The first characterization includes finding modes of the resonator. For the microstrip line resonator integrated with a 4-branched microfluidic channel, first mode of the device is at 1.49GHz and second mode is at 2.97GHz, and quality factors are 54 and 48, respectively [30]. Quality factor is the ratio between stored energy over dissipated energy, and characterizes as the name implies, quality of the resonant platform.

For the tracking of the resonance frequencies of the first and second modes in real-time, a system is constructed. This system is based on two digitally controlled signal generators and two lock-in amplifiers [30]. In the system, signal generator generates the electrical signal in the waveform, and lock-in amplifiers basically extract amplitude and phase of the signal, even in a noisy environment.

The measurement setup consists of two parallel circuits with microwave components as Power Splitter, RF Switch, Power Combiner, and Mixer. The circuit itself can be examined at Figure 2.2. In this figure, 'w' denotes the first mode frequency, and '2w' denotes the second mode frequency of the microwave resonator. Lock-in Amplifier frequencies are indicated to simplify the circuit; to make the task of the microwave components explicit. Power splitter takes one input signal and dispatches multiple output signals, which are isolated from each other, and have equal amplitudes. It can be used in reverse, to be Power Combiner. RF Switch is used to obtain the modulated Δw frequency, which is taken from Lock-in Amplifier, in TTL signal form. Mixers basically multiply two signals, a

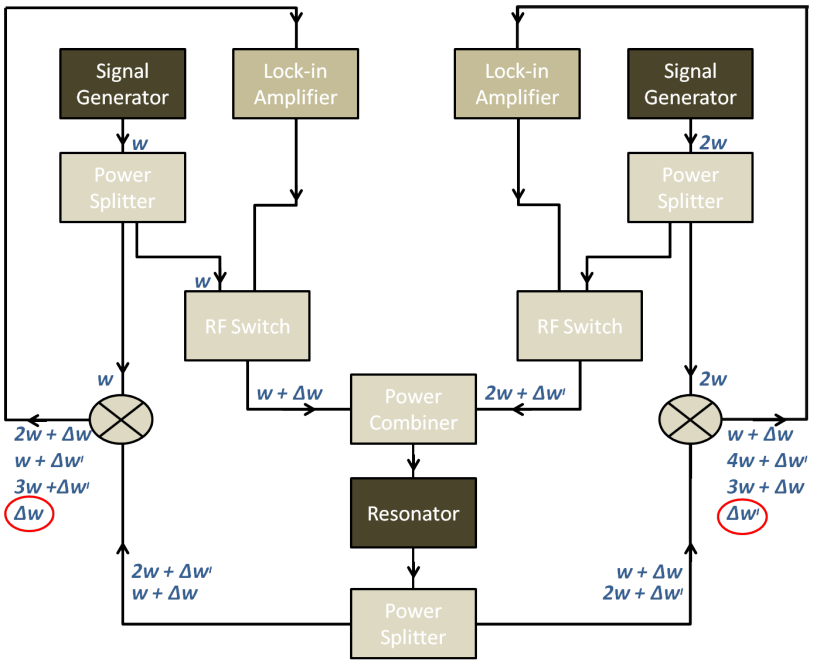

Figure 2.2: Schematic of the circuit which is used for simultaneous two modes tracking of the microwave resonator.

non-linear process, and are important at signal processing. It can be taught as the outcome of the mixer will be signals with different frequencies. Finally, a low pass filter, or a band-pass filter, (according to the lock-in amplifier frequency), can be used just before the lock-in amplifier input, to make the signal less noisy.

At resonance frequencies, the phase of the resonator is locked at 0°. Deviation from 0° (for example, due to the passage of an analyte from the microfluidic channel embedded inside the microwave resonator) creates an error signal. This error signal is used the update the frequency, and the update mechanism is based on a PI-Controller (Proportional-Integral Controller).

$$u = K_p e + K_I \int e d\zeta \tag{2.16}$$

In the setup, two parallel phase-locked loop(PLL) systems are used. It is basically an update mechanism with a feedback loop. In this work, at Chapter 4, (where water microdroplet passages create error signal) and Chapter 5, (where

single cell passages create error signal), experiments that use this measurement setup are explained. In summary, VCO routes signal to the resonator, and a phase shift will be produced. If the produced phase is not the same with the reference phase, the error signal will arise. This error signal is used to keep the frequency (that is send from the VCO) at the same value.

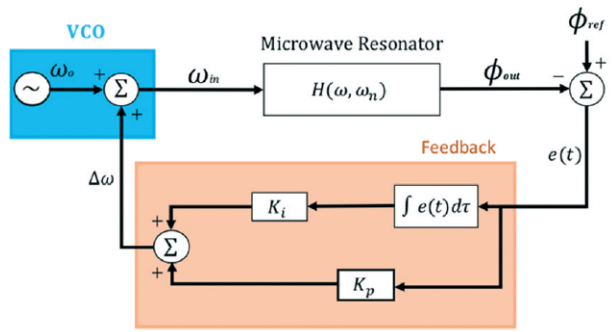

Figure 2.3: Schematic of PLL circuit; measurement system for each mode. Reprinted with permission of Royal Society of Chemistry, Lab on a Chip Journal, Issue 3, 2018.[30]

Chapter 3

Fabrication of Microstrip Line Resonators with Microchannels

Fabrication of the devices mentioned in this chapter can be divided into two subgroups: The first part involves fabrication in cleanroom. Cleanrooms are places used for micro-nano fabrication, since they are standardized and regulated in the means of particle count in the room, pressure and temperature levels, to avoid any contamination on chips. The cleanroom used to fabricate these devices is at UNAM, National Nanotechnology Research Center, where is located at Bilkent University. The second part involves fabrication in the lab environment. Some parts as the microchannels of the devices are fabricated in cleanroom, and integration part takes place in the laboratory.

3.1 Sample Preparation

Fabrication starts with cleaning the sample; Silicon wafer. This step can include RCA, or Piranha cleaning. They are used to clean organic residues and they are especially recommended before a high temperature processing. Another method is sequentially washing-off the sample with acetone, IPA (isopropanol alcohol)

and DI water, and blow drying with Nitrogen gun. To get rid of the humidity, the sample is baked at 120°C for 1–3 minutes. For the mentioned devices in this section, sequential cleaning is used.

Fabrication of the microfluidic devices are adapted from microelectronics fabrication. Usually fabrication steps include lithography, etching, and deposition. Since microfluidic applications usually take place in closed volumes, processed samples should be bonded as well. This bonding step can be challenging due to alignment, temperature levels of the process, and the need for expensive equipment. Researchers tried to come up with a low cost, rapid fabrication method, which is summarized in the next sections.

3.2 Soft Lithography

Soft lithography, a method transfers a pattern to an elastomeric stamp is commonly used for microfluidic devices. Namely, soft lithography uses flexible organic molecules, where rigid inorganic materials are used for fabrication of microelectronic systems[33]. For the referred devices, PDMS, polydimethylsiloxane, is used as the elastomeric material, due to its cheapness and practicality. PDMS offers some other unique properties as good chemical stability, being inert, nontoxic, biocompatible, optically transparent[34]. Additionally, it can be bonded to itself, or various other materials as glass slides by air or oxygen plasma[35]. It has some downsides as the absorbtion of drugs and small molecules[36]. For transient cell signalling, PDMS does not cause biological problems; however, for long term applications as cell culturing on chip, it might not be preferred.

There are maskless methods that are involved in soft lithography, as 3D-printing, laser micromachining, and microelectrical discharge machining[34], but the devices that are fabricated for the experiments are made by using the following steps.

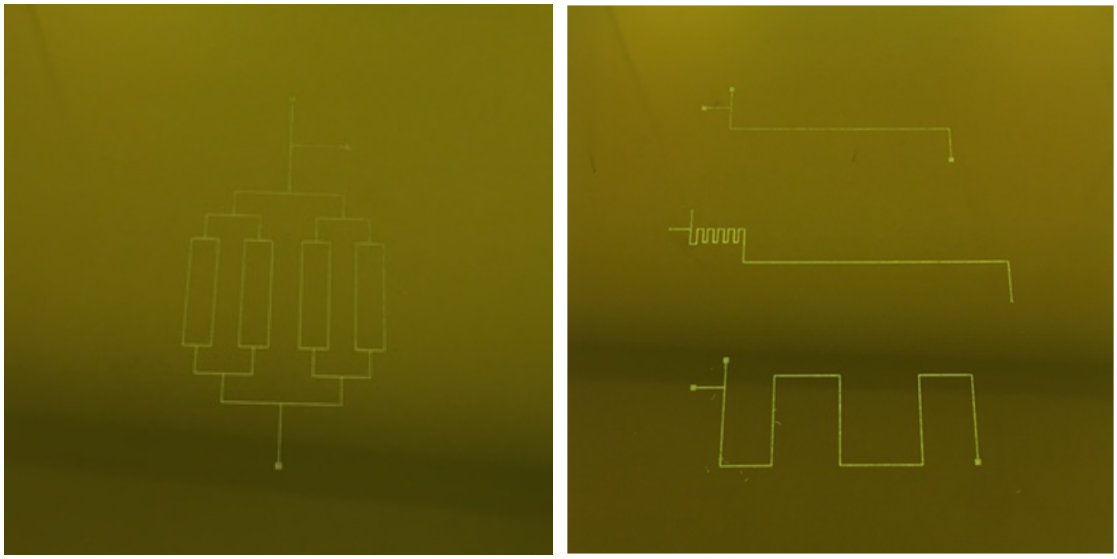

(a) Photomask for 8-branched microchannels.

(b) Photomask with single channels, different geometries.

Figure 3.1: Photomasks for microfluidic applications.

3.2.1 Mask Preparation

Photomasks, are usually made of transparent fused silica with a covered opaque chrome pattern, 5 by 5 inches, are used for obtaining desired shapes onto samples by using photolithography. Transparent sections allow UV light to pass through the sample. For this specific case, desired shapes are microchannels with different dimensions. They are prepared to obtain specific microfluidic applications, which are elucidated in the following sections, by using SOLIDWORKS and GDSII editor, namely K-layout, and taking into consideration the equipment limitations.

3.2.2 Preparation of the Master

Samples which are used as molds, usually referred as the *Master*, can be obtained by using negative photoresists, namely SU-8. Depending on the viscosity, there are different types of SU-8s that are commercially available. SU-8 used in the experiments is 2050, to obtain microchannels with different dimensions; $75\mu m$

– 200μm in depth, 30μm – 200μm in width. First, a layer of HMDS, Hexamethyldisilazane, is spin coated with following parameters, Table 3.1, to form an adhesion layer between silicon wafer and the SU-8. SU-8 is spin coated in two steps, due to its viscous nature.

Table 3.1: Spin Coating Parameters for 200μm Resist

HMDS	4000 rpm	40 seconds
SU-8	500 rpm	10 seconds
SU-8	1000 rpm	30 seconds

For different devices, different thickness of SU-8 is also tried. Some of the devices are done with 75m thickness of SU-8, and spin coating parameters can be found at table3.4.

Table 3.2: Spin Coating Parameters for 75μm Resist

HMDS	4000 rpm	40 seconds
SU-8	500 rpm	10 seconds
SU-8	2000 rpm	30 seconds

After the spin coating process, there might be build up of the photoresist on the edges of the wafer. This excess photoresist should be removed by the help of acetone; to prevent the contamination of the hot plate during baking process. Additionally, this excess photoresist affects the homogeneity of the layer; which results with uneven exposure at the photolithography step. This process is also known as Edge Bead Removal.

In order to dry the coated resist and make it more resistant, soft bake step is needed. For viscous resists as SU-8, two step baking that is elevated is recommended. Baking time and temperature can be seen from Table 3.3.

3.2.2.1 Photolithography

After negative photoresist is spin coated onto the sample, in this case silicon wafer, photolithography is used to transfer desired patterns from photomask, with UV light. It has different pattern transferring techniques: First one is when the mask is in direct contact with the substrate. The second and preferred one for this fabrication is when there is a small proximity distance between the mask and the substrate, to avoid sticking between surfaces. Since the minumum feature size is in microns, it does not result in low resolution. The light changes photoresist's chemical properties, and depending on the photoresist; negative or positive, the section of the photoresist that is exposed to light strengthens or loosens the bonds between their molecules.

In the case of SU-8, negative photoresist, exposure cross-links the bonds (Figure 3.2). Some parameters that are used for photolithography application can be seen from Table 3.3.

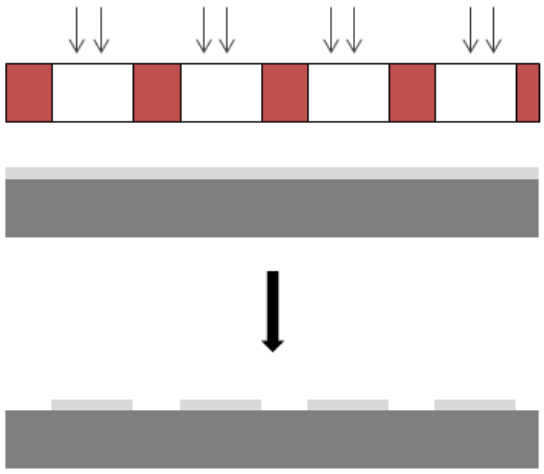

Figure 3.2: Schematic of photolithography onto negative photoresist.

In addition to silicon, other materials as glass, pyrex, or silicon nitride can be used with different exposure doses.

For $75\mu m$ thickness of SU-8, photolithography parameters can be observed at Table 3.4.

Table 3.3: Photolithography Parameters

Soft Bake	65°C, 7 minutes	95°C, 33 min
Exposure Type & Dose	Proximity	$275\frac{mJ}{cm^2}$
Post Exposure Bake	65°C, 5 minutes	95°C, 13 min

Table 3.4: Photolithography Parameters for $75\mu m$ thickness of SU-8

Soft Bake	65°C, 3 minutes	95°C, 9 min
Exposure Type & Dose	Proximity	$200\frac{mJ}{cm^2}$
Post Exposure Bake	65°C, 2 minutes	95°C, 7 min

After exposure, SU-8 layer must be heated again. This step is known as post exposure bake, and it is needed to accelerate the SU-8 polymerization. This step also reveals if the exposure is optimal or not, since visible latent image should be seen in the film after it is placed on the hotplate. Parameters can be seen from Table 3.3.

When the patterns are visible, SU-8 should be developed to form final structure. This development can take place in commercially available SU-8 Developer, or diacetone alcohol; one of the solvent based developers. Depending on the thickness of the SU-8, development times may vary, and should be optimized. The time interval used for this work is approximately 16 minutes, and constant agitation is recommended. If the pattern has tight pitch or holes, ultrasonic bath may be used during development.

Final step in the cleanroom is curing the SU-8, also known as hard bake. This step is usually recommended for devices that will be subjected to thermal processing, since SU-8 is a thermal resin and its properties can change when exposed to high temperature levels. Baking for a couple of minutes at 150°C can strengthen the structures, hence it is useful for microfluidic applications.

In the cleanroom, not only 8-branched and single zigzag microchannels are fabricated. For different applications where small channel dimensions are needed, a single channel with a smaller width for particle experiments is also established.

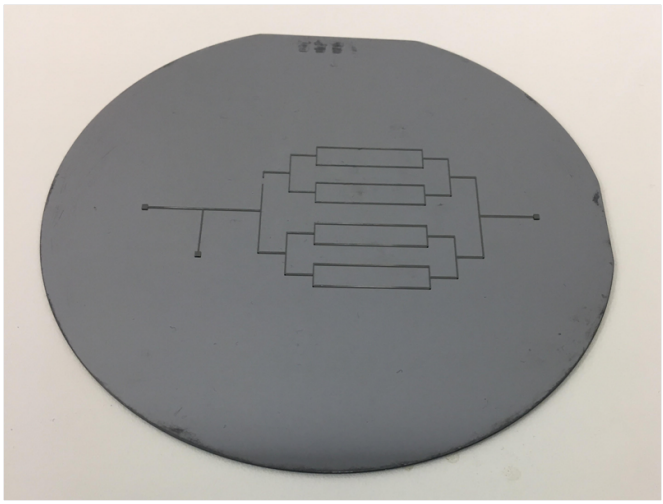

Figure 3.3: Si wafer with SU-8 structures; in this case a 8-branched microchannel. To use only 4-channels, a portion of SU-8 is removed from the mask.

Figure 3.4: Si wafer with SU-8 structure; namely a single microchannel geometry. Width of the channel is approximately $50\mu m$.

As it is explained, in addition to silicon, other materials can be used with different exposure doses.

3.2.3 PDMS Preparation

After the SU-8 master is ready to use, sample is taken to laboratory to work with PDMS. This section can also be done in the cleanroom. PDMS is prepared by using Sylgard 184 Silicone Elastomer Kit, which also contains curing agent. By changing the ratio between the elastomer and the curing agent, desired Young's Modulus, E, can be obtained. For this work, (10:1) is used. After the mixture is ready, it is put into vacuum desiccator to remove bubbles. These bubbles can solidify in the baked PDMS. Mixture is then poured onto the silicon wafer with SU-8 features,(where these features are the microchannels),and put in the oven

for 60 minutes, at 80°C, for cross-linking. Some of the PDMS that is prepared in this step is reserved to be used for the cooper sheets. The mixture can also be left at the room temperature for 24 hours.

When the PDMS is cooled down, it can be cut from the master wafer with a scalpel, and gently peeled off.(Figure 3.5) As it is explained above, this PDMS now has the microchannels that are needed to be bonded to form enclosed volumes. Since it is desired to add and remove fluids from the channels, inlet and outlet ports should be punched. The number of these ports can vary depending on the application. Due to the fact that PDMS is a soft material, ports can be gently punched out by using stainless steel punchers.

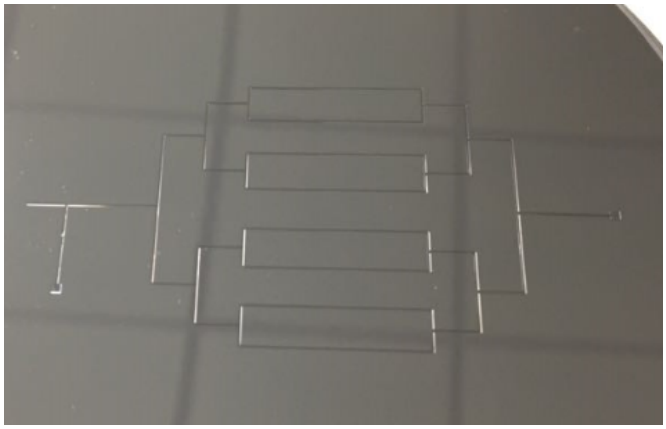

Figure 3.5: Silicon with SU-8 structures. A thin layer of PDMS is poured and baked.

3.2.4 Ground & Strip Layers

Ground and strip layers of the device is cut from a copper sheet, with a thickness of 500μm. Both layers are cut with guillotine shears, The ground plate has dimensions as 7cm x 10cm, and the strip is 0.1cm x 11cm. These parts are then polished, and ground layer is coated with the reserved PDMS, to form a thin layer, and baked.

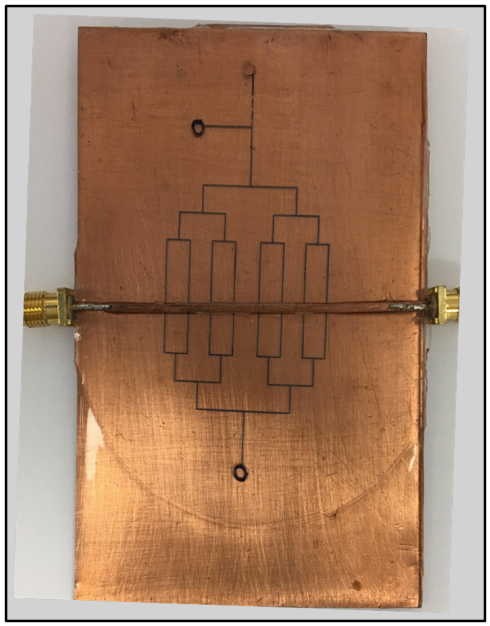

(a) 8-branched device after the microstrip line connection.

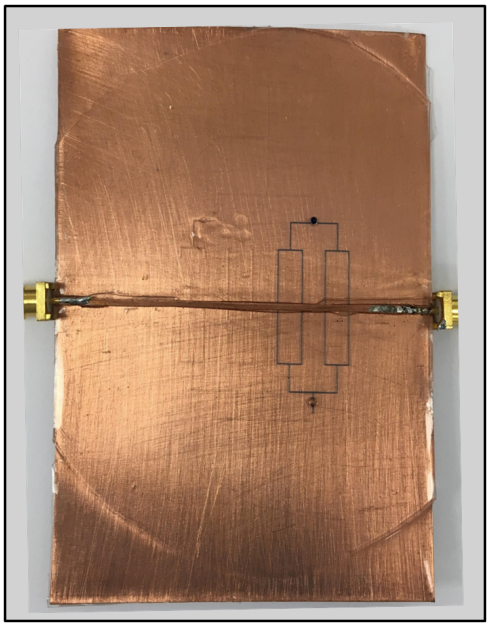

(b) One of the 4-channel branched devices.

Figure 3.6: Final products for different applications. Coloured DI water is filled in order to embellish the microchannels.

Device assembly is needed to form closed micro structures with specific volumes. In this work, plasma-activated bonding is used. It is a low temperature bonding technique and makes surfaces hydrophilic, namely the surfaces to be bonded will have similar characteristics, and removes contaminants.

After the ground layer is cooled down to room temperature, it is placed in air plasma chamber with the PDMS that has microchannel structures. Approximately in 40 seconds, air plasma activates both surfaces. After activation process, both surfaces are carefully aligned and gently pressed together. Next, copper part that will serve as the microstrip line is aligned at the center of the device and attached to the device by using PDMS as adhesive layer. Finally the end product is baked in oven for 45 minutes. Fabrication steps can be also seen from Figure 3.7.

To have electronic connection; actuation and read-out, microstrip line is bent down from both sides, touched to the ground layer. The device is grounded to

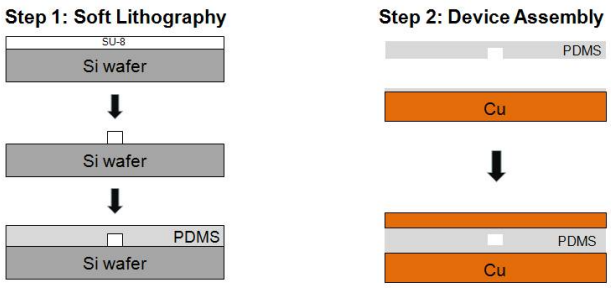

Figure 3.7: Fabrication schematic of the device.

obtain a specific boundary condition hence to have a specific mode shape, which is explained at the previous chapter. SMA ports are soldered from both sides of the device.

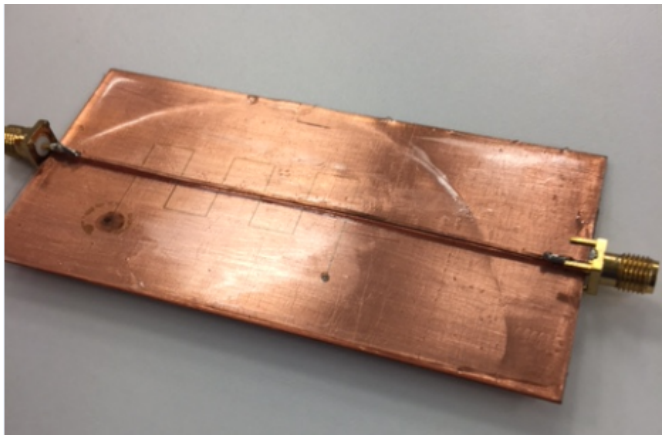

Figure 3.8: Final product for a device with a zigzag microchannel.

To deliver and collect fluids, inlet and outlet ports are used. There are two main approaches that are used for these applications. The first one is using capillary tubing (OD: $360\mu m, ID : 160\mu m$). As it can be seen from Figure 3.9, some of the devices have inlet and outlet ports for capillary tubing connections. These ports are placed with Epoxy, and the device is left at the room temperature for 24 hours.

Other method is using PTFE tubing, (OD:1.2mm). For PTFE tubing, there is no need to have other parts as connectors, it can directly be used with PDMS based devices. In general, for droplet experiments, capillary tubing is used; and

for cell experiments, PTFE tubing is used.

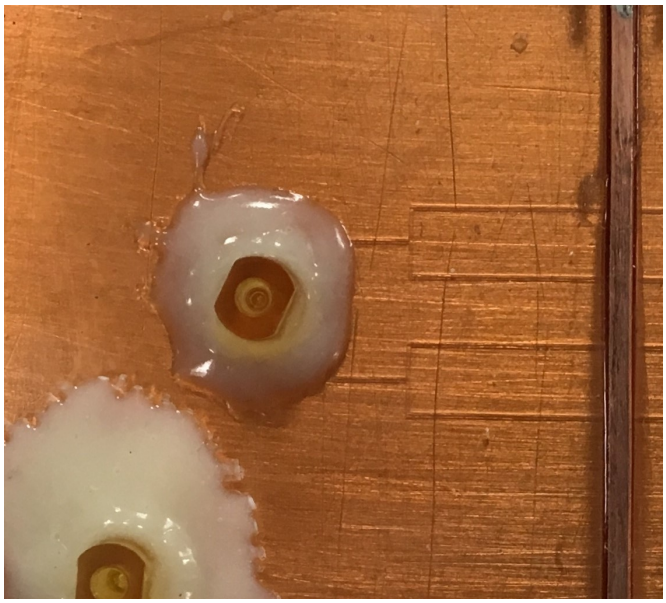

Figure 3.9: Port connector with epoxy. 4 branch of microchannels and microstrip are also visible.

Chapter 4

Droplet Detection with Microstrip line Resonator

As it is introduced at previous chapters, Lab-on-a-Chip applications gain importance due to their capability of performing chemical, biological and nanotechnological applications within small volumes. This chapter introduces droplet microfluidics, and how it is used with microstrip line resonators integrated with microfluidics.

In this work, microdroplets are formed and used in the experiments with microstrip line resonators, for size and position determination. To do the experiments, two microchannel models are used: The first channel design is based on a zigzag channel; where channel crosses signal line at 6 different locations. The second channel design is branched channels into 4, in order to sort droplets; in other words, send the droplets from different channels that are at different locations, by using hydraulic resistance. This part of the work will be investigated in the following sections.

4.1 Droplet Microfluidics

Droplet microfluidics is one of the main approaches that manipulates fluids at miniaturized platforms to perform mainly biological and chemical applications. Droplets are formed by two immiscible fluids, in laminar flow regime[37]. These manipulations take place in microdroplets, where their dynamical properties as the temperature, position and concentration must be maintained. For chemical experiments, it is favorable due to the fact that droplets can be manipulated independently and thus serve as individual reaction units[38]. It has also usage in cell and synthetic biology, due to high throughput. Cells can be loaded into droplets, and applications as cell counting or cell manipulation can be achievable. Other techniques as using microwells with a picoliter volume can also be adapted. However, these approaches can be difficult due to capillary effects at small dimensions[39]. Integration with other fields, especially cell biology makes droplet microfluidics more favourable. In this study, T-junction method is used to produce water droplets in oil. Here, oil is used for the continuous flow, and water is used for the disperse flow. For microfluidics applications, flow rate of the continuous flow is at most upto $50\frac{\mu L}{min}$. There are some parameters that are involved with droplet generation, and they are introduced briefly at upcoming sections.

To prevent droplets to merge into one, a chemical called surfactant can be added to the continuous phase, to minimize the surface tension. For this work, surfactant is not used.

Since the continuous fluid is chosen to be oil, and water droplets should not wet the channel walls, hydrophobic walls are needed.

4.1.1 Capillary Number

During droplet formation, most important forces are viscous force, and interfacial tension. Capillary Number, Ca, is a quantity that compares strength of viscous

force to interfacial force, surface tension. It should be monitored to gain a sight about the droplet dimensions, and formation rates [38].

$$Ca = \frac{\mu v}{\gamma} \tag{4.1}$$

Where μ is the viscosity and v is the velocity of the continuous fluid, γ is the surface tension between two phases.

There are three flow regimes, based on Capillary number. First regime is known as squeezing, where Ca is low. The second one is dripping regime, where viscous shear force dominates tension, and droplets are formed before disperse phase moves to the junction area. The final regime is the jetting, where Ca is high, and it seems as the disperse phase elongates along the channel for a portion. In this work, flow rates are determined in order to obtain single, rather slow droplet to track the frequency shift that is caused by this droplet, while it is passing under the signal line.

4.1.2 Flow Rate Ratio

In order to obtain homogeneous droplets with same sizes, the ratio between the flow rate of the continuous phase to disperse phase is important. To cite an example, for a large flow rate ratio and large flow rate of the disperse phase, the droplet can be in the jetting regime, which results in a large droplet, and many small droplets. In order to decide the ratio, firstly, a set of simulations are done. At the end of the simulations, flow rate of the oil (continuous phase) is decided to be greater than the water (disperse phase). A more delicate adjustment is done by experimental trials hence, flow rate ratio is determined by the end of these trials (Table 4.1). Since single droplet is needed to travel the microchannel before disturbance of other droplets, flow rates are rather slow.

Table 4.1: Flow Rates of the Continuous and Dispersed Flows

Continuous Flow($\frac{\mu L}{min}$)	Dispersed Flow ($\frac{\mu L}{min}$)
0.5	0.05
0.6	0.03
0.5	0.1
0.9	0.2

4.1.3 Geometry

Geometry of the channels is important, since it will directly affect the size of the droplets. For example, with the same flow rates and ratio, with smaller widths, smaller droplets will be formed, compared to wider channels. Another thing is that, with smaller channel dimensions, hydraulic resistance will be higher, which causes droplets to flow through other inlet; rather than the channel that will lead to outlet port.

4.1.4 T-Junction for Droplet Formation

Another geometric concern is the droplet formation junction. Droplet formation can be classified into coflow, cross-flow, and flow-focusing categories[40]. One of the methods to form droplets is using so called T-junctions, one of the cross-flow junctions. In this work, it is preffered, and schematic can be seen at Figure 4.1. This junction produces droplets hydrodynamically. To deliver oil and water and form droplets, two syringe pumps are used. Two different flows meet at an angle[41], usually this angle is orthogonal. Droplets are formed as described: Disperse phase, blokes the continuous phase, forms shear gradient, and it is broken into droplets.

Although T-Junction is one of the most used geometry to form droplets, there are other geometries for different applications as K-Junction[42], V-Junction[43].

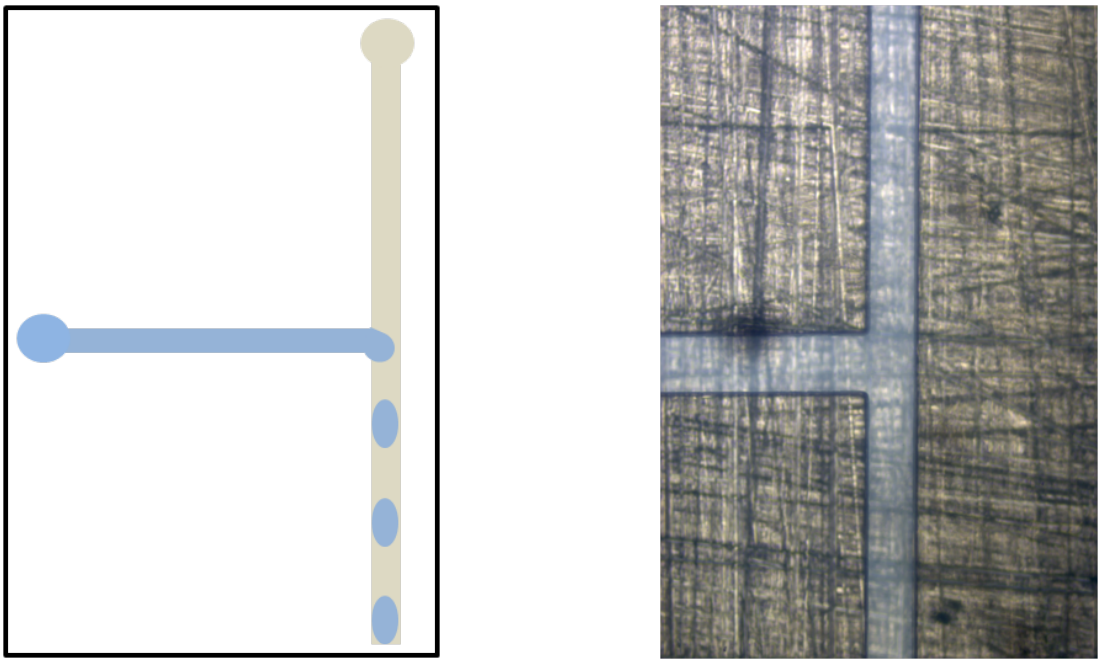

(a) Schematic. (b) Microscope image.

Figure 4.1: T-Junction for droplet formation. Water droplets are formed with carrier fluid, oil.

In this study, it is chosen since it is easy to fabricate, and it can produce monodisperse droplets.

There are also active methods to form droplets, where external forces are applied. There are electromechanical, magnetic and thermal methods. One of the methods is called as EWOD, Electrowetting-on-Dielectric, where electrical field is applied to reduce the contact angle between the flow and the channel[44].

4.2 Droplet Detection with a Zigzag Microchannel

To send microdroplets which are formed in a T-Junction, a Zigzag channel geometry is used. The reason to use such a geometry is due to the fact that microchannel crosses signal line at 6 different positions. At each position, frequency shifts on

considered modes, first and the second modes for this case, will differ, and they can be seen at Figure 4.2. One of the reasons that causes frequency shifts is the difference between the relative permittivity of the water(approximately 78.3 [45]), and the olive oil(approximately 2.5 [46]) at microwave frequency band, room temperature. Each crossing point is labelled from A to F, and the total length of the device is 99.79mm. Point E is approximately at the center of the device. The positions of the crossings are given at Table 4.2.

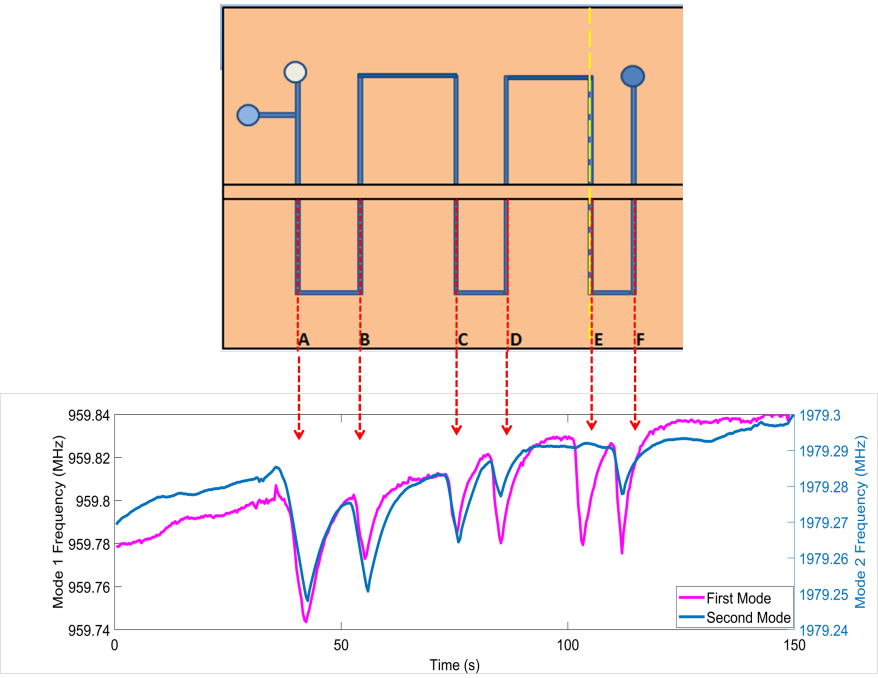

Figure 4.2: Frequency shifts on first and second modes due to droplet passage. Point E is approximately at the center of the device.

A single water microdroplet in olive oil is formed and send to the microchannel by syringe pumps. The flow rates for disperse and continuous flows are $Q_{water} = 0.03\frac{\mu L}{min}$ and $Q_{oil} = 0.6\frac{\mu L}{min}$. These rates are set after the channel is filled with water, manually, so that a slow single droplet can be formed.

Table 4.2: Normalized Positions of the Microchannel Sections Where They Cross the Signal Line.

Point A	Point B	Point C	Point D	Point E	Point F
0.192mm	0.277mm	0.36mm	0.438mm	0.518mm	0.599mm

4.3 4-Branched Microchannels for Droplet Distribution, Location and Electric Volume Calculations

The reason to use 4-branched microchannel is to sort droplets; namely distribute them into different channels. It is necessary for selection and segregation of droplets; and this system can be used for further analysis[47]. For the mentioned work, since each channel crosses the signal line at different positions, this concept is needed to test the multimode sensing for position characterization[30], (Figure 4.3). There are mainly two sorting mechanisms: Active and passive. One of the main active methods is using electrophoresis[48]. In this work, passive sorting due to hydraulic resistance is investigated.

As is stated above, due to hydrodynamic resistance that is caused by the channel geometry and passage of the earlier droplets, 4-branched channel structure is used. Resistance analogy is similar with electrical circuits, whereas the flow rate is similar to current, pressure difference replaces voltage difference, and hydraulic resistance is similar to the resistance of an electrical circuit.

$$\triangle P = QR_{hydraulic} \tag{4.2}$$

After a set of experiments, it is seen that droplets are dispersed almost randomly through the channels[30], Figure 4.3. Channels are labelled from A to D, where channel D is at the center of the microwave resonator. Histogram of the droplets can also be seen at Figure 4.3. The histogram is plotted by using 121 droplet passages, and it can be seen that channel B is less favourable than other channels. The reason for that is the fabrication defect: Channel B already has more resistance than the other channels, due to excess SU-8.

Frequency shifts that are originated from droplet passages are visible in Figure 4.3. Due to their location, each droplet creates different frequency shifts. For example, a droplet that passes through channel D, the channel which is located at the near-center of the device, induces different frequency shifts on both modes.

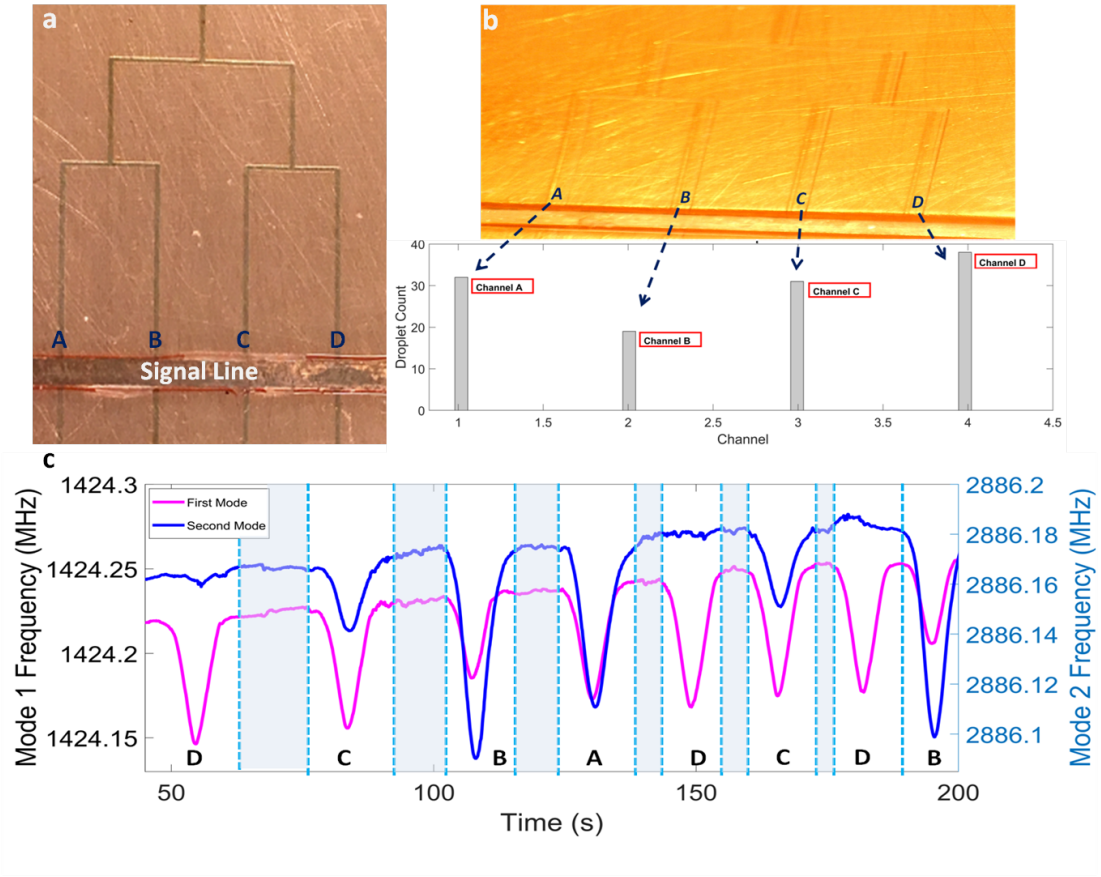

Figure 4.3: (a)4 microchannels that are used for droplet distribution. (b)Histogram of 121 droplets and their choice of microchannels. (c)Frequency shifts on both modes, due to droplet passage from one of the channels, A to D.

The reason for this is due to the fact that the amplitude of the electric field for the first mode is high at the center and second mode has antinode at the same location (due to their mode shapes and boundary conditions).

The path that the droplets follow can be examined from Figure 4.4. In this figure, a junction that is divided into two channels and 2 droplets that are consecutive can be seen. The first droplet, indicated with black circle, favours the least resistive path. Since the first droplet increases the hydraulic resistance, the second droplet, indicated with red circle, goes towards the other channel; which has lower hydraulic resistance. Therefore, only one microdroplet passes through the sensing region of the sensor, at any given time [30].

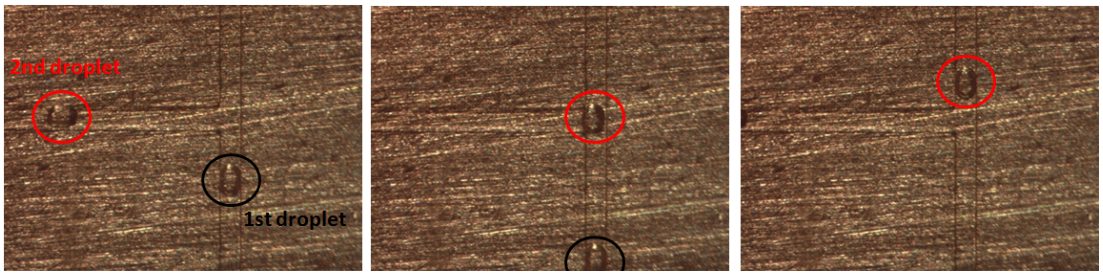

Figure 4.4: Droplet sorting by branching the microchannels. Two droplets are visible. Second droplet favours channel with lower hydraulic resistance.

The normalized locations of the channels with respect to the length of the resonator are 0.297cm, 0.365cm, 0.426cm and 0.493cm. These locations can be calculated from frequency shifts, as can be seen at Figure 4.5. For the study, they are measured beforehand the experimental trials, and compared with the results. When the frequency shifts on both modes are plotted, position values can be found as straight lines that pass through origin. Each position has different lines with different slopes [30],[20]. Additionally, position histogram can be examined for the comparison between actual and experimental data, at Figure 4.6. After location data is obtained, electrical volume of the droplet can also be calculated.

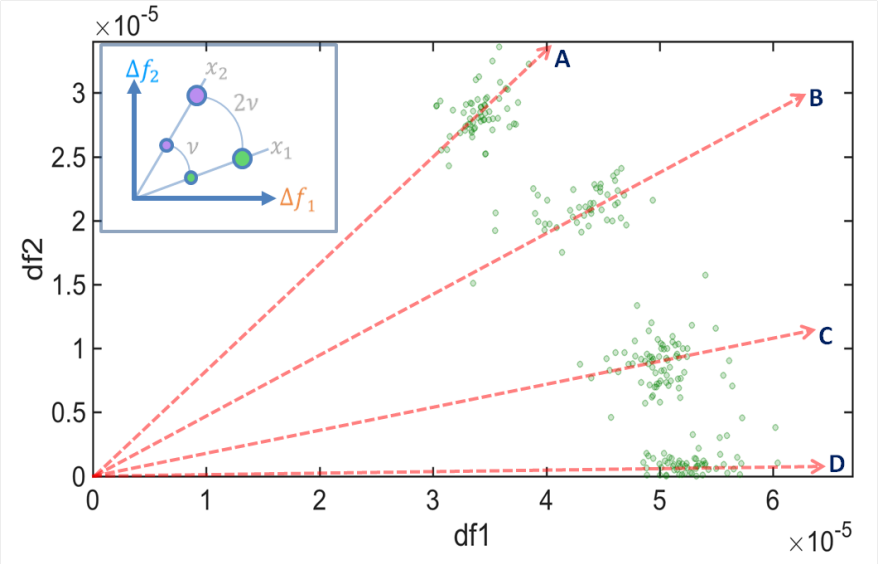

Figure 4.5: Position data of the droplets in frequency shift domain. Inset also shows how position and electrical volume contours are calculated. Reprinted with permission of Royal Society of Chemistry, Lab on a Chip Journal, Issue 3, 2018.[30]

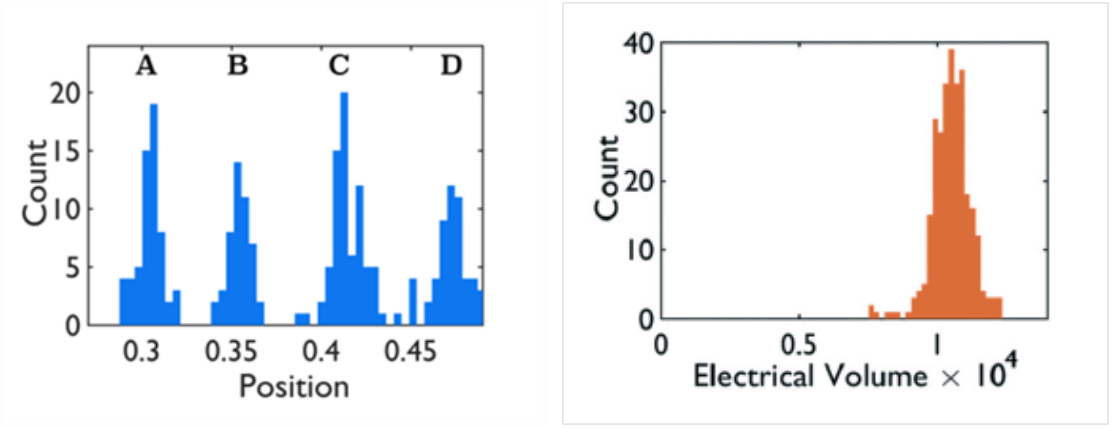

(a) Position histogram.

(b) Electrical volume histogram.

Figure 4.6: Droplet information. Reprinted with permission of Royal Society of Chemistry, Lab on a Chip Journal, Issue 3, 2018.[30]

As evident from Figure 4.6, even though droplets pass from different microchannels, electrical volume histogram has a sharp peak. The reason for this is the fact that the produced droplets have similar sizes. Size can be calculated from the electrical volume; it is the volume of the droplet times the dielectric constant difference between the continuous flow and the droplet[30]. Hence, droplets which pass through different channels indeed have the same electrical volume properties.

Chapter 5

Cancer Cell Detection & Differentiation

Novel fabrication techniques and studies on microfluidics enable Lab-on-a-Chip devices to become more useful for biological and chemical applications. As the literature review at Chapter 1 reveals, these devices can be used for single cell characterization and analysis. These analyses are important for example for drug susceptibility analysis, early detection of tumour cells, understanding cell-to-cell interactions and cell-to-extracellular matrix interactions.

Back in 1951, Dr. Gey was one of the first MDs who was trying to create immortalized cell lines, in order to find therapies for cancer. However, in vitro culturing of cell lines did not show any results, since growing human cells in laboratory usually ended up with the death of cells, after few generations. Until one patient, Henrietta Lacks, who has adenocarcinoma of the cervix and was treated by Dr. Gey. Her immortal cells, (being immortal is attributed to the ability of being cultured in laboratory environment, fast growth, and continuous divison) will be known as HeLa (named after the two first letters) [49]. In this work, HeLa cells are used to characterize their passage from the sensing region, and electrical volume. The cells are cultured at UNAM, and taken to the laboratory to obtain measurements.

Breast cancer cells can be classified as heterogeneous, and there are ongoing studies for almost 60 years to understand these cells at molecular level. Classifications can be done by the cells receptors, tumour grade, and human epidermal growth factor (HER2) [50]. Breast cancer cells are characterized by the specific cells in the breast that are affected. There are various types of breast cancer cells. To give some examples, the available cells from Bilkent University Molecular Biology and Genetics Department were: T47D, MCF-7, MDA-MB-231, MDA-MB-468, SK-BR-3 and MDA-MB-157. In the experiments, MDA-MB-157 human breast carcinoma cells are used due to their stellate structure, size and cell-to-cell interactions.

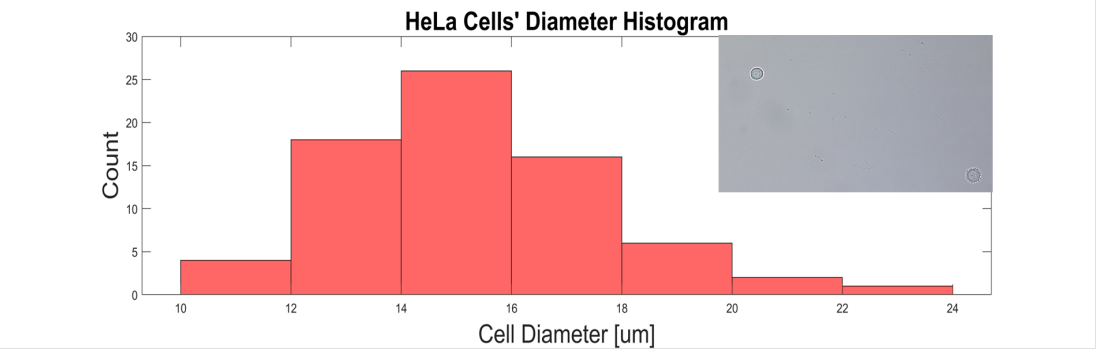

Figure 5.1: HeLa cells' histogram. Inset image shows microscopy image of HeLa cells.

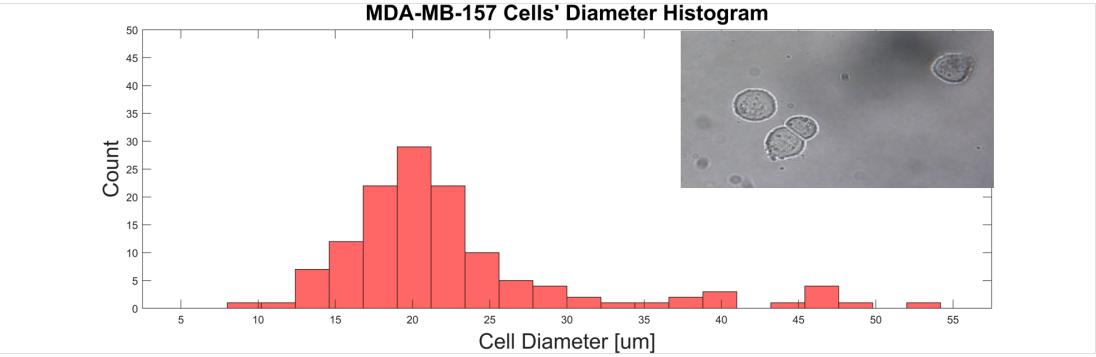

Figure 5.2: MDA-MB-157 cells' histogram. Inset image shows microscopy image of the same cells.

Optical microscopy histograms can be seen at Figure 5.1 and Figure 5.2. In order to take images of the cells, a small volume of cells, approximately $10\mu l$, is placed between two glass slides. Hence, this technique for imaging does not

provide 3-dimensional data; rather, the cells are compressed between these slides, and the deviation of the diameter values are due to this compression. Additionally, some of the cells were about to get divided, and this growth before the divison cause a few diameter values to be approximately two times the average value.

Cells are delivered to the sensing region by microfluidic set-up. The flow rate is calibrated such that in the optimal situation, only one cell travels underneath the microstrip line. The microstrip line has a width of approximately $1mm$. If the same device which is used for droplet detection is used for cell experiments, cells generally only flow through one of the channels, which is the least resistant one. The hyraulic resistance of the channel can be approximated as:

$$R_{hyd} = \frac{12\mu L}{wh^3} \tag{5.1}$$

Where L is the length of the channel, μ is the viscosity, w and h are the width and height of the channel cross-section; and $w > h$.

The approximate hydraulic resistance is $9.96 \times 10^{12} \frac{Pa.s}{m^3}$. In the first period of the experiments, only a syringe pump is used, and flow rate is chosen between $0.5 - 10 \frac{\mu L}{min}$, in order to obtain a valid pressure difference to deliver the cells. The concentration of the cells is chosen between $100.000 - 500.000 \frac{cells}{mL}$. In the optimal case, concentration of $100.000 \frac{cells}{mL}$ with a flow rate of $0.5 \frac{\mu L}{min}$ should give one cell at a time. However, due to Poiseuille Flow, where the velocity of the flow is not the same across the microchannel (velocity is at its max at the center, and approximately zero near channel walls), optimum case was difficult to achieve. Therefore, during experimental trials, some large frequency shifts, greater than one cell's capability of inducing a frequency shift, are observed.

The second part of the experiments are done with *Elveflow Pressure Controller*, OB1, where flow rate of the system is calibrated through the pressure value, which is decided by the operator, using the hydraulic resistance formula.

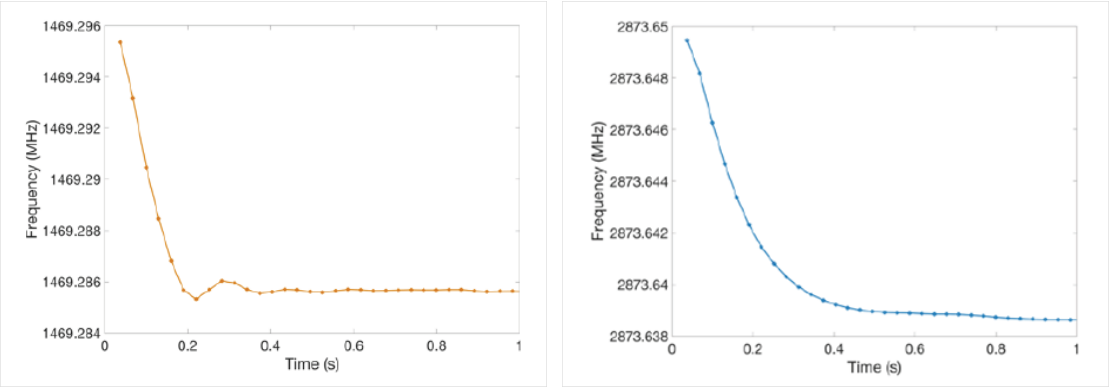

(a) First mode. (b) Second mode.

Figure 5.3: Control runs for Allan Deviation calculations. Response time of both modes can be observed. Reprinted with permission of Royal Society of Chemistry, Lab on a Chip Journal, Issue 3, 2018.[30]

5.1 Cell Detection

With the idea of microwave imaging measurement setup, which are introduced at Chapter 1 and Chapter 2, cell detection can be achieved. When a cell passes through the sensing region, in this case in a microchannel underneath the microstrip line, it induces frequency shifts on both modes. The entrance and exit of single cells can be characterized by these frequency shifts, which are distinguishable from the noise levels. The stability of the both modes are investigated by Allan Deviation measurements. Frequency drifts did not affect this stability, since it is mainly involved with the noise level in the measurement.

In this work, Allan Deviation is calculated by driving the system from approximately 10kHz offset, measuring the time response, (namely how well the PLL recovers 0° phase condition), and plotted on a log-log domain, in order to get the results. For the first and second modes of the device, Allan Deviation plots can be examined. Allan Deviation for the first mode is 1.5×10^{-8} and the second mode is 1.8×10^{-8}; and the response time is 400ms [30].

As it can be seen, with frequency values on the order of GHz, according to the Allan Deviation, the minimum measurable frequency would be between $10 - 100Hz$. Taking into consideration that frequency shift that is caused by a single

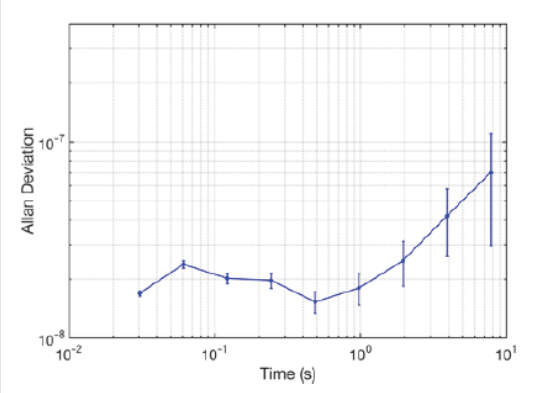

(a) First mode.

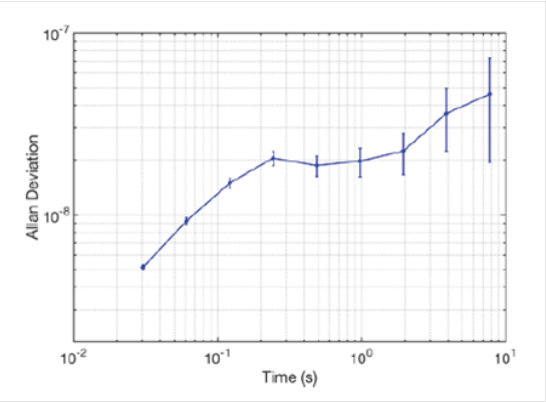

(b) Second mode.

Figure 5.4: Allan Deviation plots for the first and second modes. Reprinted with permission of Royal Society of Chemistry, Lab on a Chip Journal, Issue 3, 2018.[30]

cell passage is around $1 - 3kHz$, singal-to-noise ratio will be high in a way that sharp peaks of shifts can be detected. Additionally, signal-to-noise ratio can be calculated from the ratio between single frequency shift and noise. As it can be seen from Figure 5.5, frequency shifts caused by HeLa and MDA-MB-157 cells are around $1kHz$(Figure 5.6).

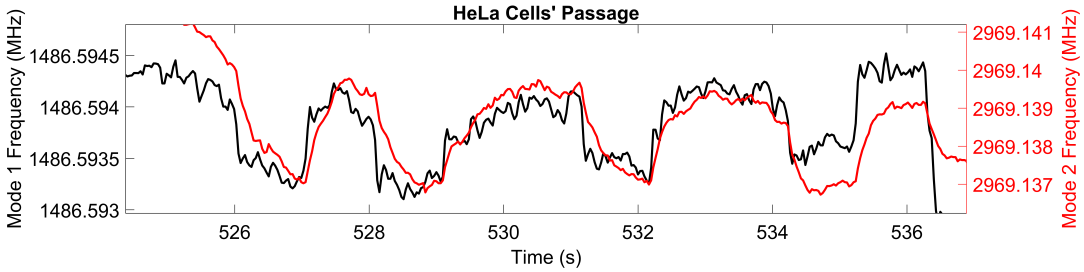

Figure 5.5: Frequency shifts on both modes due to HeLa passage.

To calculate the signal-to-noise ratio of both modes, single frequency shift can be taken into consideration. For the MDA-MB-157 cells; first mode is shifted 430Hz, where its value is 1.493GHz and Allan Deviation is 1.5×10^{-8} as stated above. Therefore, the noise level is around 22.395 Hz for the first mode. The ratio between the frequency shift and the noise level is 19.2. For the second mode, frequency shift due to single cell passage is around 800Hz, where its value

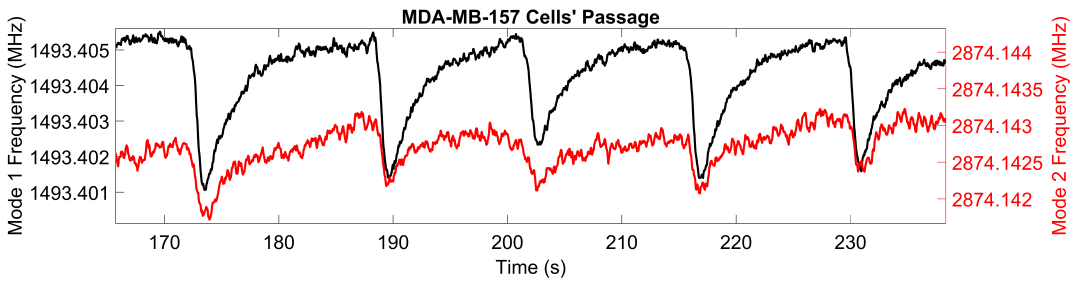

Figure 5.6: Frequency shifts on both modes due to MDA cells' passage.

is 2.875GHz and Allan Deviation result is 1.8×10^{-8}. Thus signal-to-noise ratio of the second mode is around 15.46.

When there is more then one cell underneath the signal line, frequency shift value gets larger. The reason for this is the fact that more then one cell means more permittivity change. It can be seen from Figure 5.7 the frequency shift on first mode is around 2kHz and on second mode is around 1.5kHz.

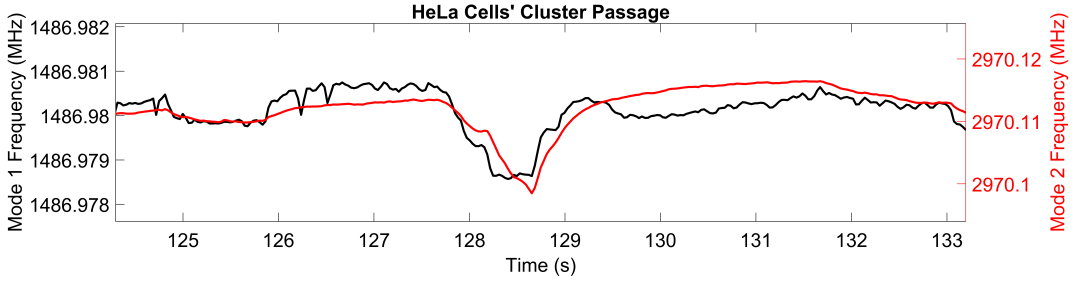

Figure 5.7: Frequency shifts on both modes due to a group of HeLa cells.

5.1.1 Electrical Volume Difference

Electrical volume calculations for analytes passing through microchannels underneath microwave resonators' sensing regions, while they are tracked by their first two modes are explained at Chapter 2. As it can be expected, electrical volume of the cells are much smaller than microdroplets, and the comparison of HeLa cells with microdoplets can be seen at Figure 5.8.

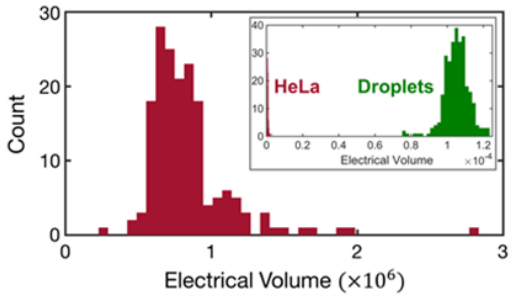

Figure 5.8: Electrical volume histogram of HeLa cells and microdoplets. Outliers indicate entry of multiple cells into the channel at the same time. The inset compares the size of the HeLa cells to the size of the microdroplets.

After the electrical volume comparison of HeLa cells to microdroplets, MDA-MB-157 cells are also used to obtain comparison between two different lines of cells (Figure 5.9).

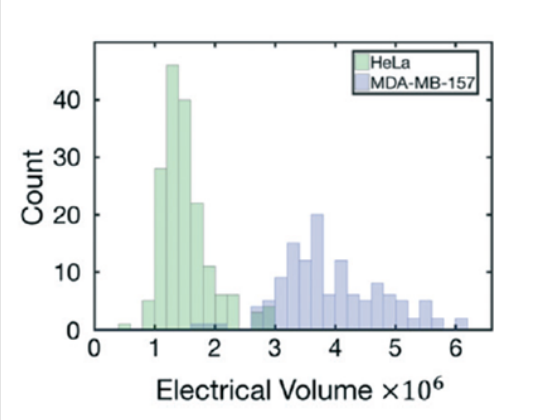

Figure 5.9: Electrical volume comparison of the HeLa and MDA-MB-157 cells. Reprinted with permission of Royal Society of Chemistry, Lab on a Chip Journal, Issue 3, 2018. [30].

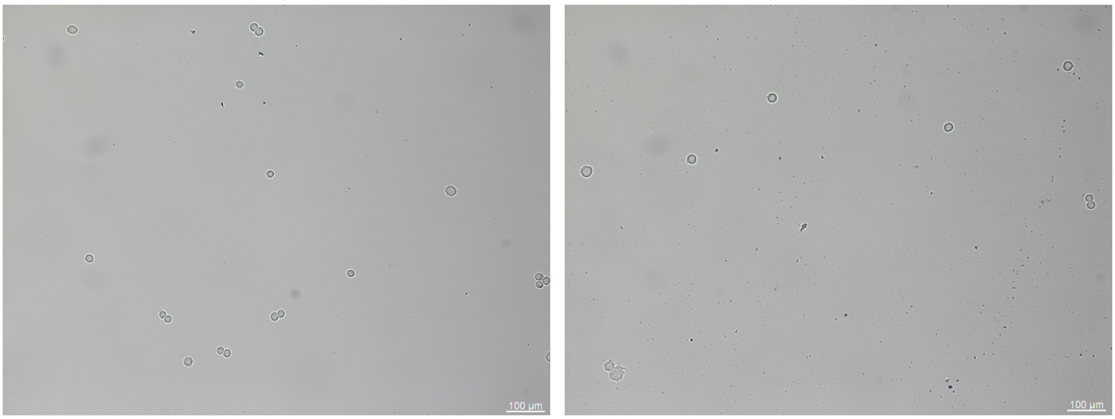

(a) Drug resistant (b) Wild type

Figure 5.10: Optical microscopy images of breast cancer cells.

5.2 Wild Type and Drug Resistant Breast Cancer Cells

Personalized cancer treatment is an ongoing research as it is explained before; for example measuring the mass accumulation rate of tumour cells to understand the drug sensitivity of every patient [17]. In the presented work, wild type and treated breast cancer cells are tried to be compared. This time, BT-474 cell line is used. As in the case of MDA-MB-157 cells, they are adherent, epithelial cells, and they can be used to study herceptin resistance. Wild type refers to the cells that are not treated. Treated cancer cells are given different drugs, in order to investigate their drug resistance. Unfortunately, the size of the cells were similar, in a way that they cannot be differentiated by two-mode measurements. Yet, by using higher order modes simultaneously, they can be differentiated in the future.

In summary, with microwave resonators integrated with microfluidics, cell detection and differentiation can be achieved. In this study, by using the first two mode of a microstrip resonator, label-free and real-time detection of HeLa and MDA-MB-157 cancer cells are done. The important part is to have different cells with different sizes. However, by using higher-order modes simultaneously, more information about the analytes such as their composition, can be obtained.

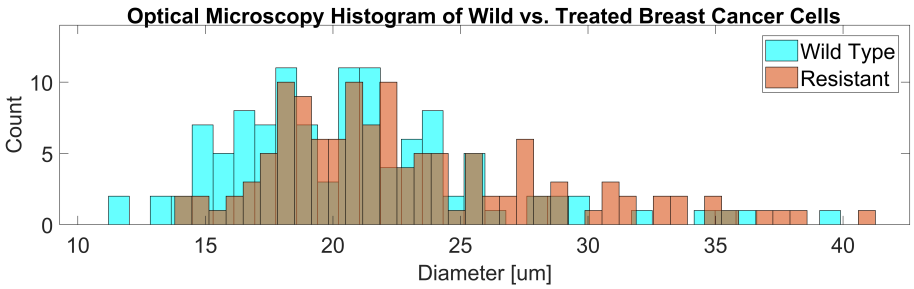

Figure 5.11: Size comparison of wild type and treated breast cancer cells. Since they are similar in size, it is difficult to compare their electrical volume.

Chapter 6

Novel Facile Resonators

In this thesis thus far, microstrip resonators with micrfluidic channels are investigated. These channels were embedded inside PMDS, a material that is widely used for microfluidic applications due to its characteristics as being low-cost, biocompatible, porous, and easy handling. However, PDMS is not the best material for applications in the microwave domain. One can use material properties as dielectric constant and loss tangent to choose a dielectric material for specific applications. Dielectric constant, also known as relative permittivity, is a measure of the loss of microwave energy, relative to the energy at free space. Loss tangent, also known as dissipation factor is related to the loss of energy, and it is a factor of frequency.

PDMS has loss tangent of 0.07 [51] at the lower spectrum of the microwave regime. Another material, Kapton, type of a polymide film, which was developed by Dupont, has some advantageous characteristics. For example, it has a dissipation loss approximately 0.008 around $1GHz$, at room temperature [52].

Additionally, thickness of the PDMS is another limitation with these kind of devices. The non-uniformity of the thickness will cause lower quality factors, since it will cause non-symmetrical structures, due to fabrication errors. Another thing is, thick dielectric materials could lower the signal that would be induced

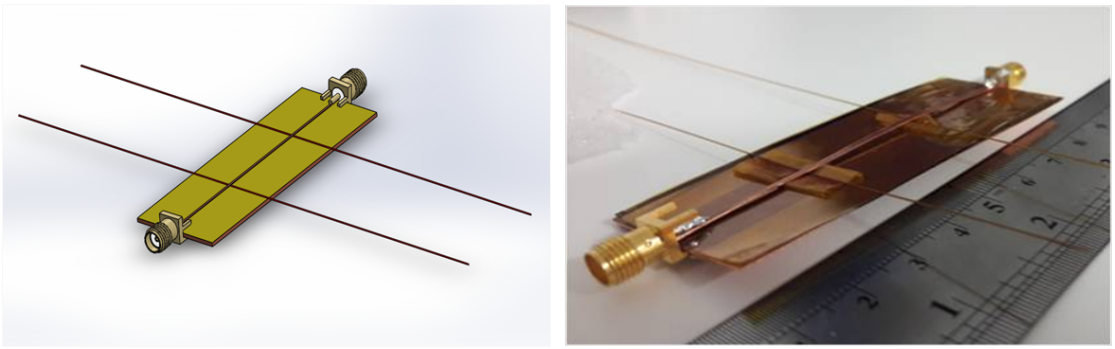

(a) Design of the microstrip line resonator. (b) Picture of preliminary kapton device.

Figure 6.1: Microstrip line resonator with Kapton and capillary tubings.

from the passage of the analyte, due to the electric field in sensing direction.

In this chapter, low cost resonators rely on Kapton as the dielectric material are introduced. The thickness of the Kapton is $25\mu m$. In order to deliver biological analytes as cells, capillary tubings (OD : $360\mu m$, ID : $100\mu u$) are used. With this technique, low-cost and rapid devices can be obtained.

The quality factor of this new device which is based on Kapton is around 130, whereas the device which is based on PDMS is 54, both for the first modes of the devices.

6.1 Fabrication

In the fabrication process of devices based on Kapton, clean room equipments are not used. A copper plate is cut to be the ground layer, and thin Kapton film is placed on top of it. 2 capillary tubings are placed symmetrically, approximately at the 33% and 66% of the plate, and fixed by kapton tapes. On top of the device, microstrip line, with a width of 1mm and thickness of 0.5mm is placed. Finally, SMA connections are done by welding, a process which is explained at the Fabrication Chapter. This kind of a fabrication process provides low-cost, and rapid production. Resulting preliminary device can be observed at Figure 6.1.

6.2 Cell Experiment

With these new type of resonators, SK-BR-3 breast cancer cells are delivered to the sensing region, in order to prove the concept. Again, microstrip line resonators are used with 2 capillary tubings, which are placed symmetrically, at the approximately 33% of the device. In these experiments, due to device limitations, only the first mode of the device is tracked, while cells are being delivered underneath the microstrip line, inside a capillary tube. The first mode of the device is $2041.137MHz$, and the second mode is approximately the double of this value. Hence, due to the frequency limitation of the signal generators in the laboratory, only the first mode is used.

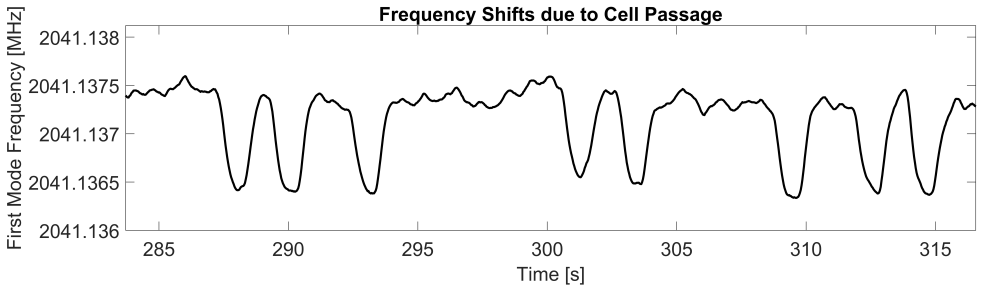

Figure 6.2: Frequency shifts on first mode due to single cell passage events.

As it can be observed from PLL of the first mode, a single cell causes approximately $1kHz$ frequency shift. Allan Deviation is measured to be around 2×10^{-8}. Hence the noise floor of the first mode is around 40Hz. This will lead up to a signal-to-noise ratio of 25; which is higher than the devices based on PDMS's signal-to-noise ratio (Figure 6.3).

With approximately 96 events, cell passages underneath the signal path, frequency shifts on the first mode can be observed at Figure 6.4.

In summary, new and facile devices; instead of PDMS based for the dielectric and therefore the microfluidic part, which are based on Kapton and capillary tubing are fabricated. As a proof-of-concept, first mode is tracked and frequency shifts due to breast cancer cell passages recorded. These new kind of devices offer

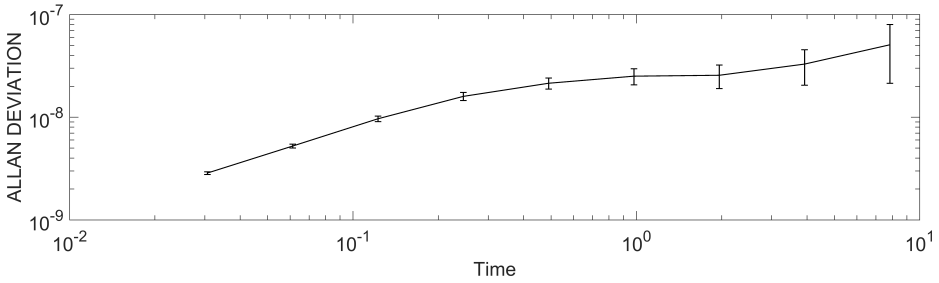

Figure 6.3: Allan Deviation of the first mode.

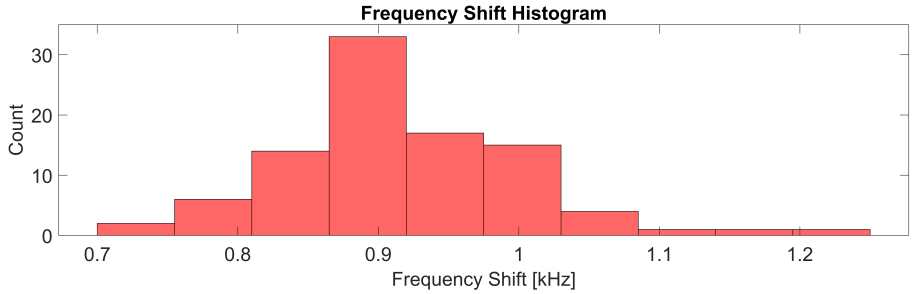

Figure 6.4: First mode frequency shift histogram.

low cost, rapid; one device approximately takes 20 minutes to be produced, and higher quality factor and thus signal to noise ratio characteristics. With higher-order modes and simultaneous tracking, more information about analytes can be obtained.

6.3 Kapton Etch Trials

Since Kapton is a replacement with good characteristics, in order to eliminate the need for capillary tubing, etching Kapton is tried, to obtain microchannels.

In order to obtain microchannels with small dimensions as $20\mu m$ to observe cell behaviour, and make thinner dielectric material, kapton is etched with different maskings. Thin layer of dielectric material is needed for electrical field.

First step is cleaning the Kapton with IPA, rinsing with DI water, and blowing with dry nitrogen. After cleaning, A layer of kapton is placed on top of a silicon

wafer to provide a rigid layer. Adhesion layer is done by coating SU-8, $40\mu m$. When the kapton is placed, it is baked for 5 minutes at 120°C, and 2 minutes at 150°C.

First trial for masking is done with SU-8 as the masking material. $40\mu m$ SU-8 is coated on top of kapton layer, and spin coating parameters can be seen at Table 6.1. Soft bake times are 65°C for 3minutes, 95°C for 7 minutes. It is left at room temperature for one day.

Table 6.1: Spin Coating Parameters for 40μm Resist

HMDS	4000 rpm	40 seconds
SU-8	500 rpm	10 seconds
SU-8	4000 rpm	40 seconds

In order to obtain patterns for etching, photolithography is used with $180\frac{mJ}{cm^2}$. Post exposure bake is done with 65°C for 2 minutes, and 95°C for 6 minutes. Development takes place in SU-8 developer after the wafer is cooled down, approximately for 7 minutes. To have structural rigidity, hard bake is done for 2 minutes at 150°.

Inductively Coupled Plasma, ICP, is used for etching, with SF_6 and O_2 gases (45:15, 200W). Its working mechanism depends on creation of plasma, which is done by a varying electric current, and magnetic field. First etching trial is done for 10 minutes, and it is extended to 30 minutes. SF_6, Sulfur hexafluoride, is widely used for plasma since fluorine part is useful for etching and O_2 can expedite the etch rate [53]. The reason to use ICP rather than RIE is the device availability. Optical microscopy images of the etched surfaces for different time durations can be observed at Figure 6.5.

Characterization of the etch depth is done by Scanning Electron Microscopy, SEM, which is used widely for characterization in various disciplines as biology, material science etc [54]. Visualization reveals that the depth is $1 - 2\mu m$.

Since the etch depth is not enough for cell passage; and it can squeeze cells,

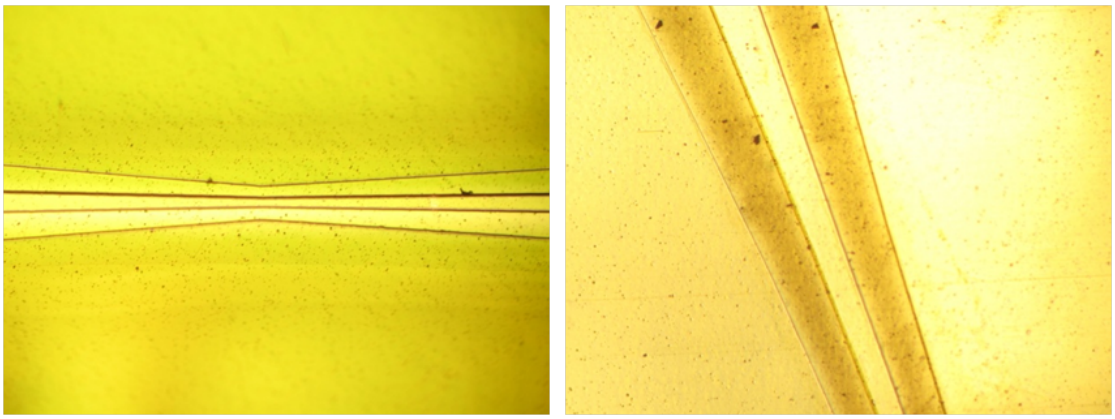

(a) Etching for 10 minutes. (b) Etching for 30 minutes.

Figure 6.5: Optical microscopy images of etching where SU-8 is used as the masking material.

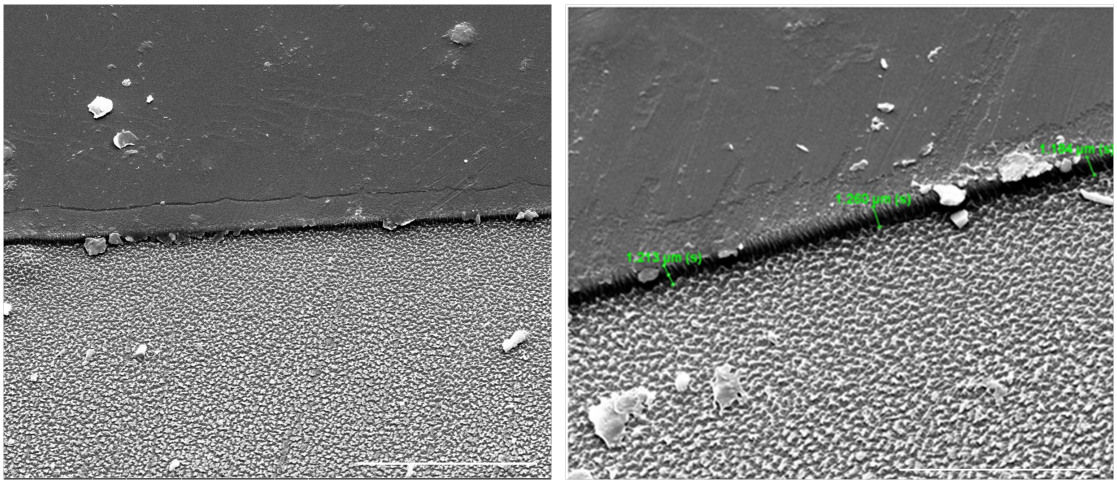

(a) Scale bar shows $20\mu m$. (b) Scale bar shows $10\mu m$.

Figure 6.6: SEM image of etching from different perspectives.

damage them and cause stress on them, another masking material is tried. This time chrome, a metal layer, is chosen to make the mask more durable under etching conditions.

Kapton is placed onto silicon wafer by 2 methods: First one is by using Kapton tape, and second one is by using AZ4562 positive photoresist as the adhesion layer. After chrome deposition, second method seems more favourable.

For patterning, AZ4562 positive photoresist is coated with 3700 rpm, for 40 seconds. It is baked for 1 minutes at 120°C. Photolithography is used for patterning with $120\frac{mJ}{cm^2}$, 200m seperation. AZ400K developer is used for development(3:7), approximately for 1 minutes.

Chrome is deposited onto Kapton layers by thermal evaporator. Thermal evaporation is one of the most widely used methods for thin layer deposition, it is one of the Physical Vapor Deposition techniques. The substrates are placed above the deposition material. This material is heated in vacuum, and by heating, atoms leave the surface, and travel through the substrate. The thickness of the coated chrome is approximately $100nm$. After deposition, Kapton layers are left at the lift-off, overnight. This lift-off process also separates Kapton from Si wafer (where photoresist is used as the adhesion layer).

After masking process, microchannels can be etched. Etching is done by Reactive Ion Etching, RIE for 90 minutes. RIE is one of the dry etching techniques, which combines chemical and physical etching, resulting with anisotropic etch profiles. SF_6 and O_2 gases are used $(25 : 10, 150W, 25mTorr)$ again. Chrome layer is wet etched by commercially available Chrome Etcher before characterization.

After the etching process, characterization is done by SEM, in order to measure the depth of the microchannels. Approximately $12\mu m$ is etched. For future fabrication processes, chrome etching should take longer time since there are visible Cr islands.

Hence, Kapton etching is tested for future cell passage experiments. Etching

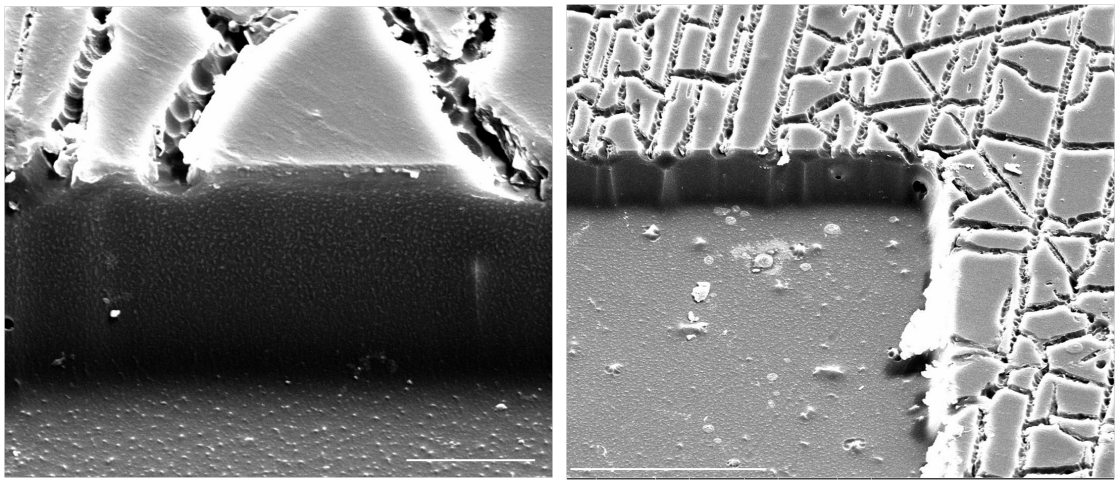

(a) Scale bar shows $5\mu m$.

(b) Scale bar shows $30\mu m$.

Figure 6.7: SEM images of etching when the chrome is used as the masking material.

for single cell passage is achieved with depth of approximately $12\mu m$. Only drawback of the process is the rough surface after etching. This roughness can deform cells, and since their three dimensional microwave imaging is the main goal, this can cause difficulties. Therefore, in the future, process should be optimized before experimental trials.

Chapter 7

Conclusion and Future Works

In this chapter, a summary of the work, and what can be done as the next steps are introduced.

As it is explained, in this work, multimode detection techniques are used in microwave domain, which are originated from mechanical domain. While the microwave resonator's higher order electromagnetic modes are tracked simultaneously, and if an analyte is delivered to the sensing region, morphological and electrical properties of this analyte can be extrapolated. To test this paradigm, a microstrip line resonator with embedded microchannels is fabricated. This resonator is tracked within its first and second electromagnetic modes, simultaneously, in order to obtain real-time and label-free detection. Position and electrical volume information about the analytes can be obtained while these analytes are passing through the microhannel, one by one, underneath the signal line. First experimental trials are done with water microdroplets inside oil flow. After the validation, two different types of cancer cells, cervical and breast, are detected, and differentiated based on their electrical volume histograms.

Prototype of devices are done with using PDMS as the dielectric material and for microchannels. First steps of the fabrication take place in cleanroom, where SU-8 master is prepared. After experiments with droplets and mammalian

cells, another device is developed. This new type of device relies on Kapton as the dielectric material, and capillary tubings for analyte delivery to the sensing region. The main difference between these materials is the loss tangent and thus signal-to-noise levels of measurements. Additionally, second generation devices does not need any cleanroom processing, they are rapid to be produced and low-cost. As a proof-of-concept, breast cancer cells are detected with second generation devices as well.

If the higher order modes are used, one can obtain more information about the analyte, such as its orientation, skewness and size. These characteristics of the analyte can be used to reconstruct the global image of it, rather than the pixel by pixel image.

For cell detection, Allan Deviation results which are lower than 2×10^{-8} are obtained. Due to characteristics of microwave domain where the difference between the indices of refraction is greater than the optical frequency domain between biological particles and medium, microwave frequency range make sensing possible.

Biological analytes that are going to be examined with optical microscopy are usually placed between two glass slides. Therefore their sizes and shapes can alter. Additionally, they can be affected by the shear stress. The proposed sensing technique exhibits no contact, hence no effect on cell's state.

This platform can be used for flow cytometry applications, extrapolating the composition of analytes, and on-chip cell culturing, at is explained in the next section.

7.1 Organ-on-Chip Platforms

A platform which mimics human pathophysiology in vitro is crucial, in order to develop personalized medicine, and disease modelling. Additionally, testing on animals has moral concerns [55].

As Lab-on-a-Chip devices, Organ-on-Chip (OoC) platforms offer interdisciplinary approaches to mimic cell culturing environments, for in vitro clinical studies. The main similarity between Organ-on-Chip platforms is the fact that these devices can mimic a specific organ, tissue, biological environment, to study the specific cell behaviours. There are different examples from various laboratories. In order to mimic such environments, mechanical forces on specific cells, extracellular matrix, cell-to-cell interactions should be taken into consideration.

These devices are favourable for therapeutic studies. As it is explained, Organ-on-Chip platforms are getting in favour worldwide. For example, as it is introduced earlier, Mass Accumulation Rate, (MAR), Analysis is being used for specifically weighing single myeloma cells, repeatedly, when treated with different drugs, namely; dexamethasone, lenalidomide, and bortezomib. The reason to measure MAR of individual cells is involved with the fact that when treated, cells without resistance to these drugs will reduce their masses[18]. In order to study cells' behaviour, long time intervals are needed. However, without mimicking their environment, cells cannot maintain their viability. Therefore, these kind of experiments need culturing conditions as maintaining 37°C, and 5% CO_2 concentration, which is established by customized OoC platform.

Another example from literature is a culturing platform, which aims to prevent the need of petri dishes, and to provide on chip long term culturing. The device is based on materials as glass and silicon. In order to provide fresh medium, nutrients, and gases, porous hydrogel membranes are used. In this platform, cells are exchanging materials by diffusion. This way, shear on cells are avoided[56]. There are other devices which let more then one cell line to be cultured, on the same platform. Extracellular matrix is chosen to be fibronectin, which coats PDMS effectively when kept at 37°C, for 30 minutes [57].

There are also more specific OOC platforms, as Heart-on-a-Chip, Kidney-on-a-Chip, or Lung-on-a-Chip, which are all mimic these specific organs, on chip. Just to give an example, back in 2010, a group from Wyss Institute at Harvard University published an article about Lung-on-a-Chip. Its working principle is based on the relation between alveolar-capillary interface of the human lung, and

they are studying the effect of nanotoxic particles[58].

As a follow up to the present work, growth of cells, specifically MDA-MB-231 breast cancer cells, can be examined. As it is known, mammalian cells have a growth cycle, which are G1/S, and G2/M, and cells will have different volumes at each phase. Additionally, specific therapeutic drugs target a particular phase. Lovastatin, one of the metabolic agents and its use for cancer therapautics has being examined, can be studied for metabolic manipulations of cancer cells. For example, Kim et al., have studied the effect of such metabolic regaents on breast cancer cells and have shown a great difference between the diameter of these cells. When cells are exposed to serum starvation, a method to make every cell in the same phase, the average diameter of cells become $18\mu m$; whereas when lovastatin is applied when cells are in G1 phase, diameter of cells are approximately $35\mu m$ [59]. In summary, with our detection mechanism, which is label-free, and real-time, these manipulations can be achieved, and tracked by multimode microwave resonator. Culturing can be done on-chip and at the same time can be monitored with microscope, which is inside an incubator. Therefore, long-term cultivation experiments, cell cycle manipulations with anticancer drugs can be done (Figure 7.1).

In summary, it is crucial to make cells maintain their viability, if long term studies are desired. Thus far in the experiments, cells delivered to the microwave resonator by syringe pump or pressure controller, and transit time is under 1 minute, for every single cell. Hence, their viability was not desired for long hours, since only their passage from the signalling area is tracked for position and electrical volume calculations. In the future applications as drug treatment and therapeutic studies, their viability becomes much more important. Their viability is achieved by making the experimental set-up mimic the biological environment by appropriate temperature, humidity, and CO_2 concentration as well as appropriate choice of extracellular matrix. Additionally, the devices that are being used for the experiments should be optimized for culturing environment. A culturing chamber is needed with microfluidic connections to both culture and

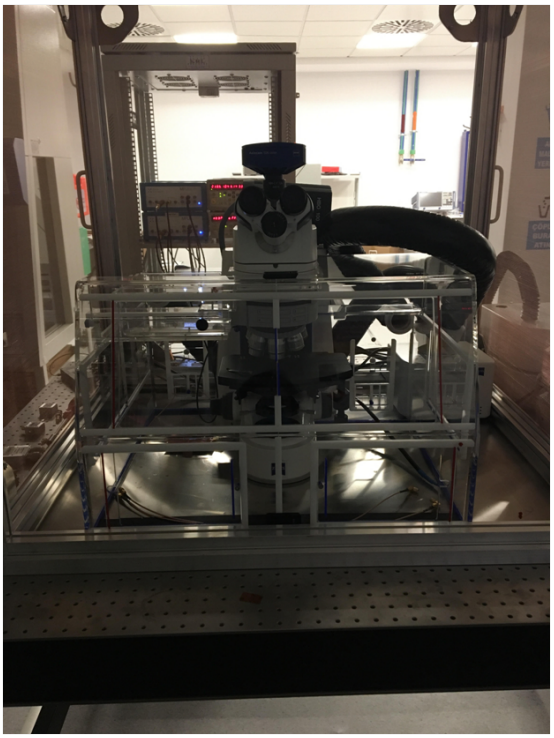

Figure 7.1: Microscope inside an incubator, surrounded by faraday cage.

deliver the cells into the sensing region; rather than only a microchannel structure. Also, for single cell studies, as investigating a drug treatment on a single cell, a zigzag microchannel structure underneath the signal line can be adopted, to get a signal from the cell, couple of times. That way, microchannel crosses signal line at various positions, and call can be sensed as a function of time and position; its response to various treatments can be sensed.

7.2 Fused Silica Device Fabrication

Due to its electrical properties at microwave regime, a fabrication flow based on fused silica is composed. Most steps in the fabrication will be done in cleanroom. Another reason to choose fused silica is due to its rigid surface, it will preserve its mechanical properties (SMA connections cannot bend edges etc.), and due to this homogeneity, noise will be reduced, resulting with high signal-to-noise ratio.

Before the fabrication process, two fused silica samples should be cleaned by Piranha solution, following acetone, IPA and DI water; N_2 blowing. After the surfaces are clean, inlet and outlet ports should be drilled to one of the samples. For the microstrip line, positive photoresist is needed to be coated (AZ4562, 3700rpm, 40seconds). After photolithography process with appropriate masking for the microstrip line, sample should be developed in AZ400K developer. Metallization process is done by coating Chrome and Gold layers, lift-off, and electroplating, if the thickness of the layer is not sufficient for application.

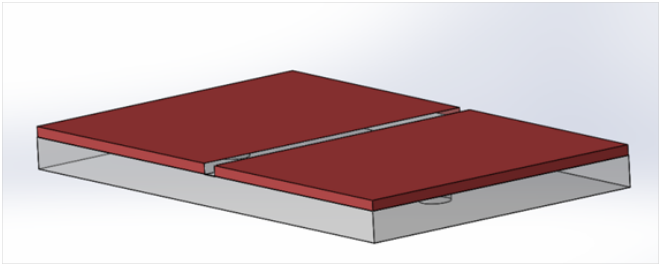

Figure 7.2: Schematic of fused silica sample after inlet-outlet openings and lithography.

On the other sample, which is cleaned before, microchannel openings can be done. For this process, SU-8 is chosen to be as the masking material, with a thickness of $75\mu m$. After photolithography and development steps, sample can be etched by dry etching, following a wet etch dipping, in order to remove any residues. On the same sample, back side should be coated with Chrome and Gold layers, in order to provide the ground layer. Finally, SU-8 residue can be removed by one of the following methods: wet polymer removal, Piranha, or O_2 plasma.

For the bonding of two layers, direct bonding method which will take place in room temperature for 24 hours can be tried. After the bonding, SMAs can be welded to two sides of the microstrip line, by using Indium-Lead solders.

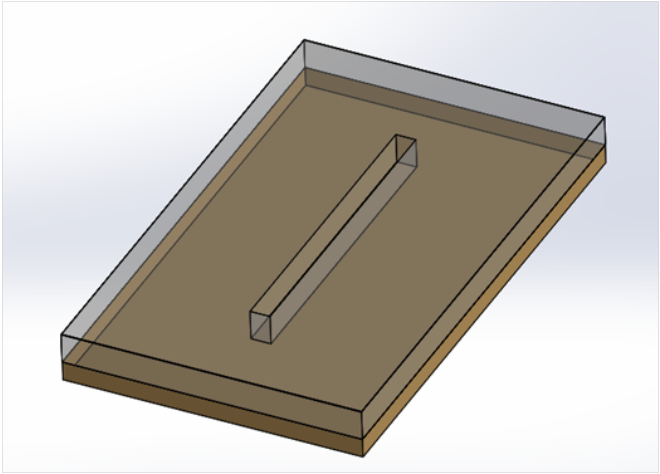

Figure 7.3: Schematic of the sample with ground layer and microchannel.

Bibliography

[1] A. Manz, D. J. Harrison, E. M. Verpoorte, J. C. Fettinger, A. Paulus, H. Lüdi, and H. M. Widmer, "Planar chips technology for miniaturization and integration of separation techniques into monitoring systems: capillary electrophoresis on a chip," *Journal of Chromatography A*, vol. 593, no. 1-2, pp. 253–258, 1992.

[2] H. P. Le, "Progress and trends in ink-jet printing technology," *Journal of Imaging Science and Technology*, vol. 42, no. 1, pp. 49–62, 1998.

[3] A. T. Woolley and R. A. Mathies, "Ultra-high-speed dna sequencing using capillary electrophoresis chips," *Analytical chemistry*, vol. 67, no. 20, pp. 3676–3680, 1995.

[4] G. M. Whitesides, "The origins and the future of microfluidics," *Nature*, vol. 442, no. 7101, p. 368, 2006.

[5] S. Takayama, E. Ostuni, P. LeDuc, K. Naruse, D. E. Ingber, and G. M. Whitesides, "Laminar flows: Subcellular positioning of small molecules," *Nature*, vol. 411, no. 6841, p. 1016, 2001.

[6] J. Krüger, K. Singh, A. O'Neill, C. Jackson, A. Morrison, and P. O'Brien, "Development of a microfluidic device for fluorescence activated cell sorting," *Journal of micromechanics and microengineering*, vol. 12, no. 4, p. 486, 2002.

[7] J. El-Ali, P. K. Sorger, and K. F. Jensen, "Cells on chips," *Nature*, vol. 442, no. 7101, p. 403, 2006.

[8] P. S. Dittrich and A. Manz, "Lab-on-a-chip: microfluidics in drug discovery," *Nature Reviews Drug Discovery*, vol. 5, no. 3, p. 210, 2006.

[9] G. Medoro, N. Manaresi, A. Leonardi, L. Altomare, M. Tartagni, and R. Guerrieri, "A lab-on-a-chip for cell detection and manipulation," *IEEE Sensors Journal*, vol. 3, no. 3, pp. 317–325, 2003.

[10] T. P. Burg, M. Godin, S. M. Knudsen, W. Shen, G. Carlson, J. S. Foster, K. Babcock, and S. R. Manalis, "Weighing of biomolecules, single cells and single nanoparticles in fluid," *nature*, vol. 446, no. 7139, p. 1066, 2007.

[11] M. S. Hanay, S. I. Kelber, C. D. O'Connell, P. Mulvaney, J. E. Sader, and M. L. Roukes, "Inertial imaging with nanomechanical systems," *Nature nanotechnology*, vol. 10, no. 4, p. 339, 2015.

[12] T. P. Burg and S. R. Manalis, "Suspended microchannel resonators for biomolecular detection," *Applied Physics Letters*, vol. 83, no. 13, pp. 2698–2700, 2003.

[13] P. Dextras, T. P. Burg, and S. R. Manalis, "Integrated measurement of the mass and surface charge of discrete microparticles using a suspended microchannel resonator," *Analytical chemistry*, vol. 81, no. 11, pp. 4517–4523, 2009.

[14] M. Godin, A. K. Bryan, T. P. Burg, K. Babcock, and S. R. Manalis, "Measuring the mass, density, and size of particles and cells using a suspended microchannel resonator," *Applied physics letters*, vol. 91, no. 12, p. 123121, 2007.

[15] A. K. Bryan, V. C. Hecht, W. Shen, K. Payer, W. H. Grover, and S. R. Manalis, "Measuring single cell mass, volume, and density with dual suspended microchannel resonators," *Lab on a Chip*, vol. 14, no. 3, pp. 569–576, 2014.

[16] N. Cermak, S. Olcum, F. F. Delgado, S. C. Wasserman, K. R. Payer, M. A. Murakami, S. M. Knudsen, R. J. Kimmerling, M. M. Stevens, Y. Kikuchi, *et al.*, "High-throughput measurement of single-cell growth rates using serial microfluidic mass sensor arrays," *Nature biotechnology*, vol. 34, no. 10, p. 1052, 2016.

[17] M. M. Stevens, C. L. Maire, N. Chou, M. A. Murakami, D. S. Knoff, Y. Kikuchi, R. J. Kimmerling, H. Liu, S. Haidar, N. L. Calistri, *et al.*, "Drug sensitivity of single cancer cells is predicted by changes in mass accumulation rate," *Nature biotechnology*, vol. 34, no. 11, p. 1161, 2016.

[18] A. E. Cetin, M. M. Stevens, N. L. Calistri, M. Fulciniti, S. Olcum, R. J. Kimmerling, N. C. Munshi, and S. R. Manalis, "Determining therapeutic susceptibility in multiple myeloma by single-cell mass accumulation," *Nature communications*, vol. 8, no. 1, p. 1613, 2017.

[19] E. Gil-Santos, D. Ramos, J. Martínez, M. Fernández-Regúlez, R. García, Á. San Paulo, M. Calleja, and J. Tamayo, "Nanomechanical mass sensing and stiffness spectrometry based on two-dimensional vibrations of resonant nanowires," *Nature nanotechnology*, vol. 5, no. 9, p. 641, 2010.

[20] M. S. Hanay, S. Kelber, A. Naik, D. Chi, S. Hentz, E. Bullard, E. Colinet, L. Duraffourg, and M. Roukes, "Single-protein nanomechanical mass spectrometry in real time," *Nature nanotechnology*, vol. 7, no. 9, p. 602, 2012.

[21] S. Stuchly and C. Bassey, "Microwave coplanar sensors for dielectric measurements," *Measurement Science and Technology*, vol. 9, no. 8, p. 1324, 1998.

[22] T. Chretiennot, D. Dubuc, and K. Grenier, "A microwave and microfluidic planar resonator for efficient and accurate complex permittivity characterization of aqueous solutions," *IEEE Transactions on Microwave Theory and Techniques*, vol. 61, no. 2, pp. 972–978, 2013.

[23] A. A. Abduljabar, D. J. Rowe, A. Porch, and D. A. Barrow, "Novel microwave microfluidic sensor using a microstrip split-ring resonator," *IEEE Transactions on Microwave Theory and Techniques*, vol. 62, no. 3, pp. 679–688, 2014.

[24] A. Ebrahimi, W. Withayachumnankul, S. F. Al-Sarawi, and D. Abbott, "Microwave microfluidic sensor for determination of glucose concentration in water," in *Microwave Symposium (MMS), 2015 IEEE 15th Mediterranean*, pp. 1–3, IEEE, 2015.

[25] K. Grenier, D. Dubuc, P.-E. Poleni, M. Kumemura, H. Toshiyoshi, T. Fujii, and H. Fujita, "Integrated broadband microwave and microfluidic sensor dedicated to bioengineering," *IEEE Transactions on microwave theory and techniques*, vol. 57, no. 12, pp. 3246–3253, 2009.

[26] A. Matsumoto and Y. Miyahara, "Current and emerging challenges of field effect transistor based bio-sensing," *Nanoscale*, vol. 5, no. 22, pp. 10702–10718, 2013.

[27] C. Laborde, F. Pittino, H. Verhoeven, S. Lemay, L. Selmi, M. Jongsma, and F. Widdershoven, "Real-time imaging of microparticles and living cells with cmos nanocapacitor arrays," *Nature nanotechnology*, vol. 10, no. 9, p. 791, 2015.

[28] M. Nikolic-Jaric, S. Romanuik, G. Ferrier, G. Bridges, M. Butler, K. Sunley, D. Thomson, and M. Freeman, "Microwave frequency sensor for detection of biological cells in microfluidic channels," *Biomicrofluidics*, vol. 3, no. 3, p. 034103, 2009.

[29] U. Kaatze, "Complex permittivity of water as a function of frequency and temperature," *Journal of Chemical and Engineering Data*, vol. 34, no. 4, pp. 371–374, 1989.

[30] M. Kelleci, H. Aydogmus, L. Aslanbas, S. O. Erbil, and M. S. Hanay, "Towards microwave imaging of cells," *Lab on a Chip*, 2017.

[31] C. Gabriel, S. Gabriel, and y. E. Corthout, "The dielectric properties of biological tissues: I. literature survey," *Physics in Medicine & Biology*, vol. 41, no. 11, p. 2231, 1996.

[32] S. Gabriel, R. Lau, and C. Gabriel, "The dielectric properties of biological tissues: Ii. measurements in the frequency range 10 hz to 20 ghz," *Physics in medicine & biology*, vol. 41, no. 11, p. 2251, 1996.

[33] Y. Xia and G. M. Whitesides, "Soft lithography," *Annual review of materials science*, vol. 28, no. 1, pp. 153–184, 1998.

[34] M. Leester-Schädel, T. Lorenz, F. Jürgens, and C. Richter, "Fabrication of microfluidic devices," in *Microsystems for Pharmatechnology*, pp. 23–57, Springer, 2016.

[35] N. Lucas, S. Demming, A. Jordan, P. Sichler, and S. Büttgenbach, "An improved method for double-sided moulding of pdms," *Journal of Micromechanics and Microengineering*, vol. 18, no. 7, p. 075037, 2008.

[36] M. W. Toepke and D. J. Beebe, "Pdms absorption of small molecules and consequences in microfluidic applications," *Lab on a Chip*, vol. 6, no. 12, pp. 1484–1486, 2006.

[37] H. Song, J. D. Tice, and R. F. Ismagilov, "A microfluidic system for controlling reaction networks in time," *Angewandte Chemie*, vol. 115, no. 7, pp. 792–796, 2003.

[38] L. Shang, Y. Cheng, and Y. Zhao, "Emerging droplet microfluidics," *Chemical reviews*, vol. 117, no. 12, pp. 7964–8040, 2017.

[39] S. Mashaghi, A. Abbaspourrad, D. A. Weitz, and A. M. van Oijen, "Droplet microfluidics: A tool for biology, chemistry and nanotechnology," *TrAC Trends in Analytical Chemistry*, vol. 82, pp. 118–125, 2016.

[40] G. F. Christopher and S. L. Anna, "Microfluidic methods for generating continuous droplet streams," *Journal of Physics D: Applied Physics*, vol. 40, no. 19, p. R319, 2007.

[41] P. Zhu and L. Wang, "Passive and active droplet generation with microfluidics: a review," *Lab on a Chip*, vol. 17, no. 1, pp. 34–75, 2017.

[42] R. Lin, J. S. Fisher, M. G. Simon, and A. P. Lee, "Novel on-demand droplet generation for selective fluid sample extraction," *Biomicrofluidics*, vol. 6, no. 2, p. 024103, 2012.

[43] Y. Ding, X. C. i Solvas, *et al.*, ""v-junction": a novel structure for high-speed generation of bespoke droplet flows," *Analyst*, vol. 140, no. 2, pp. 414–421, 2015.

[44] M. J. Jebrail, M. S. Bartsch, and K. D. Patel, "Digital microfluidics: a versatile tool for applications in chemistry, biology and medicine," *Lab on a Chip*, vol. 12, no. 14, pp. 2452–2463, 2012.

[45] C. Malmberg and A. Maryott, "Dielectric constant of water from 00 to 1000 c," *Journal of research of the National Bureau of Standards*, vol. 56, no. 1, pp. 1–8, 1956.

[46] G. Paranjpe and P. Deshpande, "Dielectric properties of some vegetable oils," in *Proceedings of the Indian Academy of Sciences-Section A*, vol. 1, pp. 880–886, Springer, 1935.

[47] A. C. Hatch, A. Patel, N. R. Beer, and A. P. Lee, "Passive droplet sorting using viscoelastic flow focusing," *Lab on a Chip*, vol. 13, no. 7, pp. 1308–1315, 2013.

[48] K. Ahn, C. Kerbage, T. P. Hunt, R. Westervelt, D. R. Link, and D. Weitz, "Dielectrophoretic manipulation of drops for high-speed microfluidic sorting devices," *Applied Physics Letters*, vol. 88, no. 2, p. 024104, 2006.

[49] W. F. Scherer, J. T. Syverton, and G. O. Gey, "Studies on the propagation in vitro of poliomyelitis viruses: Iv. viral multiplication in a stable strain of human malignant epithelial cells (strain hela) derived from an epidermoid carcinoma of the cervix," *Journal of Experimental Medicine*, vol. 97, no. 5, pp. 695–710, 1953.

[50] D. L. Holliday and V. Speirs, "Choosing the right cell line for breast cancer research," *Breast cancer research*, vol. 13, no. 4, p. 215, 2011.

[51] P.-Y. Cresson, Y. Orlic, J.-F. Legier, E. Paleczny, L. Dubois, N. Tiercelin, P. Coquet, P. Pernod, and T. Lasri, "1 to 220 ghz complex permittivity behavior of flexible polydimethylsiloxane substrate," *IEEE Microwave and Wireless Components Letters*, vol. 24, no. 4, pp. 278–280, 2014.

[52] J. Salem, F. Sequeda, J. Duran, W. Lee, and R. Yang, "Solventless polyimide films by vapor deposition," *Journal of Vacuum Science & Technology A: Vacuum, Surfaces, and Films*, vol. 4, no. 3, pp. 369–374, 1986.

[53] Y. Tzeng and T. Lin, "Dry etching of silicon materials in sf 6 based plasmas roles of and gas additives," *Journal of The Electrochemical Society*, vol. 134, no. 9, pp. 2304–2309, 1987.

[54] Y. Wang and V. Petrova, "Scanning electron microscopy," *Nanotechnology Research Methods for Foods and Bioproducts*, pp. 103–126, 2012.

[55] D. E. Ingber, "Developmentally inspired human 'organs on chips'," *Development*, vol. 145, no. 16, p. dev156125, 2018.

[56] F. Bunge, S. v. d. Driesche, and M. J. Vellekoop, "Microfluidic platform for the long-term on-chip cultivation of mammalian cells for lab-on-a-chip applications," *Sensors*, vol. 17, no. 7, p. 1603, 2017.

[57] K.-i. Kamei, H. Takahashi, C. J. Shu, X. Wang, G. W. He, R. Silverman, C. G. Radu, O. N. Witte, K.-B. Lee, H.-R. Tseng, *et al.*, "Integrated microfluidic devices for combinatorial cell-based assays," *Biomedical microdevices*, vol. 11, no. 3, pp. 547–555, 2009.

[58] D. Huh, B. D. Matthews, A. Mammoto, M. Montoya-Zavala, H. Y. Hsin, and D. E. Ingber, "Reconstituting organ-level lung functions on a chip," *Science*, vol. 328, no. 5986, pp. 1662–1668, 2010.

[59] U. Kim, C.-W. Shu, K. Y. Dane, P. S. Daugherty, J. Y. Wang, and H. Soh, "Selection of mammalian cells based on their cell-cycle phase using dielectrophoresis," *Proceedings of the National Academy of Sciences*, vol. 104, no. 52, pp. 20708–20712, 2007.

Appendix A

Cell Culture

In this part, composition of cell culturing reagents are explained, both for HeLa and breast cancer cells. Additionally, some of the crucial culturing equipments are listed.

A.1 Cell Medium Composition

For the experiments that are conducted with cancer cells, namely HeLa (cervical) and MDA-MB-157 (breast), cells are delivered to the sensing region in appropriate mediums. These mediums have similar compositions. For HeLa cells, the used media contains DMEM (low glucose without L-glutamine), 10% Fetal Bovine Serume (FBS), 1% L-glutamine and 0.5% pen/strep antibiotic. The medium for MDA-MB-157 cells is composed of DMEM (low glucose without L-glutamine), 10% FBS, 1% NEAA and 1% pen/strep. The differences in cell mediums cause no significant difference when resonance frequency of the sensor is tracked, while loaded with mediums individually.

DMEM, Dulbecco's Modified Eagle Medium, is a cell culture medium which includes various types of nutritions. Fetal Bovine Serum is a supplement for cell culture media, it is especially important for growth of cells. NEAA, non-essential

amino acids, are added to the cell culturing medium to minimize the production of these amino acids by cells themselves, since this production may harm cell growth; pen/strep, penicillin and streptomycin antibiotics, are used to prevent bacterial growth in the culture.

A.2 Cell Culturing Equipments

In order to culture mammalian cells without contamination, laboratory environment with specific regulations are needed. The first equipment is the biosafety cabinet, also known as cell culture hood. Culturing takes place in these devices with special air flow, unidirectional, with HEPA-filter. In order to mimic the tissue environment, cells should be kept at incubators with constant temperature, humidity, and CO_2 levels. For mammalian cells, temperature should be around 37°C, and CO_2 concentration should be 5%. In order to store culturing reagents, a freezer which works around -20°C is preferable. Additionally, to prevent instability of cells, another cell group can be stored in cryogenic freezer, for future studies.

Appendix B

Droplet Formation Simulations

In order to have a rationale for the flow rates to form water microdroplets in oil, a basic simulation is done by using COMSOL, Multiphase Flow Interface. In this simulation, a two dimensional version of microchannel is used, with a width of $200\mu m$. The length of the channel is arranged such that pressure difference can be achieved. There are two inlets, namely for the continuous and disperse phases, and initial condition is set such that at t=0 instant, oil is filled to all of the channel. Surface tension is chosen to be liquid-liquid interface, olive oil and water, at 20°C. This parameter can also be set manually and it is important for droplet formation. In order to solve the problem, Physically Controlled Mesh is used.

Since flow rate ratio approximates the droplet size and droplet formation regime, different flow rates are compared within the simulation. Initial conditions are given by setting the inlet velocity, rather then the flow rate, and flow rates are obtained by simply multiplying with the cross section geometry. By increasing the flow velocity of the water, droplet diameters can get greater.

The first set of trial is done by choosing $V_{water} \rangle V_{oil}$. As it can be seen from the figure, droplet with dimensions greater than channel dimensions can be formed. (Figure B.1)

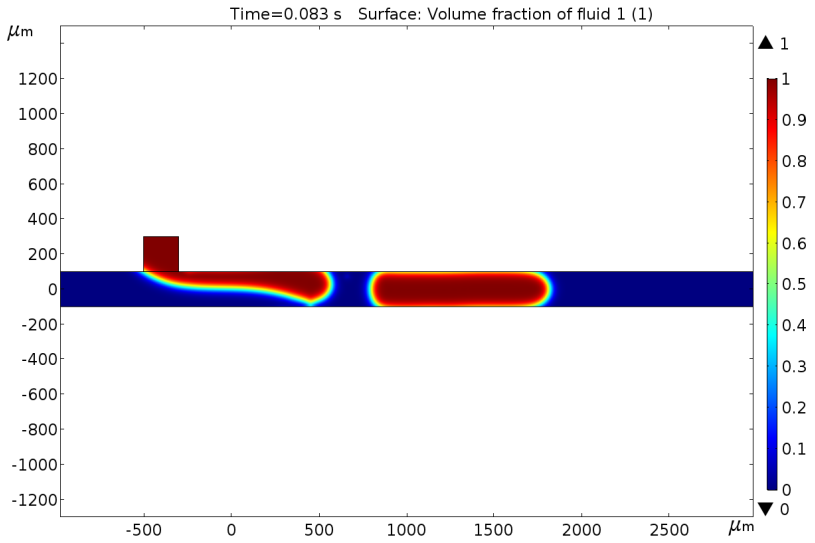

Figure B.1: Droplet formation trial while V_{water} is greater than V_{oil}.

The second trials are done with velocity conditions of $V_{water} \langle\langle V_{oil}$. As it can be seen from the figure, droplets cannot be formed, in 2 seconds. Only a thin layer of fraction of fluid is visible. (Figure B.2)

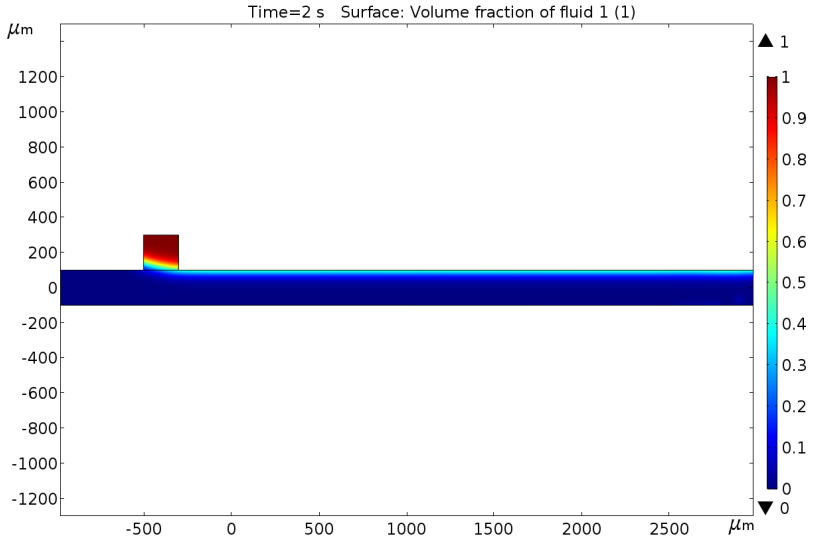

Figure B.2: Droplet formation trial while V_{water} is smaller than V_{oil}.

While the velocity of the oil is twofold the velocity of water, a simulation is constructed. $V_{water} = 0.0185\frac{m}{s}, V_{oil} = 0.037\frac{m}{s}$. Additionally, while $V_{oil} = 1.85 \times V_{water}$, droplet sizes are compared. A variation between the droplet formation locations are visible.

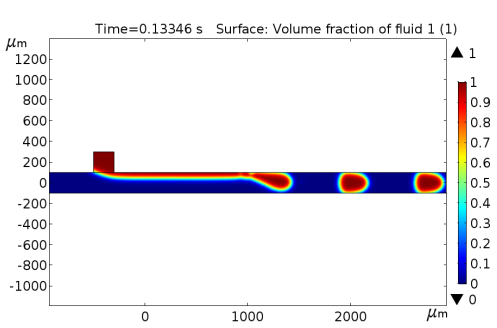

(a) $V_{oil} = 2 \times V_{water}$

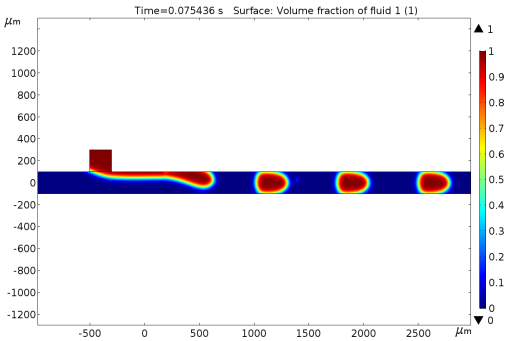

(b) $V_{oil} = 1.85 \times V_{water}$

Figure B.3: Droplet formation with different velocity ratio.

By considering the flow rate ratios which are observed by Comsol first, experiments with droplets are done. Due to resolution of syringe pumps, channel geometry and human errors, different flow rates are also tested experimentally. After simulations, flow rate ratio between oil and water is set such that Q_{oil} is greater than Q_{water}, in all experimental trials.